CANADIAN THESES ON MICROFICHE

I.S.B.N.

THESES CANADIENNES SUR MICROFICHE

National Library of Canada
Collections Development Branch

Canadian Theses on
Microfiche Service

Ottawa, Canada
K1A 0N4

Bibliothèque nationale du Canada
Direction du développement des collections

Service des thèses canadiennes
sur microfiche

NOTICE

The quality of this microfiche is heavily dependent upon the quality of the original thesis submitted for microfilming. Every effort has been made to ensure the highest quality of reproduction possible.

If pages are missing, contact the university which granted the degree.

Some pages may have indistinct print especially if the original pages were typed with a poor typewriter ribbon or if the university sent us a poor photocopy.

Previously copyrighted materials (journal articles, published tests, etc.) are not filmed.

Reproduction in full or in part of this film is governed by the Canadian Copyright Act, R.S.C. 1970, c. C-30. Please read the authorization forms which accompany this thesis.

AVIS

La qualité de cette microfiche dépend grandement de la qualité de la thèse soumise au microfilmage. Nous avons tout fait pour assurer une qualité supérieure de reproduction.

S'il manque des pages, veuillez communiquer avec l'université qui a conféré le grade.

La qualité d'impression de certaines pages peut laisser à désirer, surtout si les pages originales ont été dactylographiées à l'aide d'un ruban usé ou si l'université nous a fait parvenir une photocopie de mauvaise qualité.

Les documents qui font déjà l'objet d'un droit d'auteur (articles de revue, examens publiés, etc.) ne sont pas microfilmés.

La reproduction, même partielle, de ce microfilm est soumise à la Loi canadienne sur le droit d'auteur, SRC 1970, c. C-30. Veuillez prendre connaissance des formules d'autorisation qui accompagnent cette thèse.

THIS DISSERTATION
HAS BEEN MICROFILMED
EXACTLY AS RECEIVED

LA THÈSE A ÉTÉ
MICROFILMÉE TELLE QUE
NOUS L'AVONS REÇUE

NL-339 (r. 82/08)

Canada

32

58789

National Library of Canada / Bibliothèque nationale du Canada

CANADIAN THESES ON MICROFICHE / THÈSES CANADIENNES SUR MICROFICHE

NAME OF AUTHOR/*NOM DE L'AUTEUR* DAYAKANTHI KALUARACHCHI
(Last name)

TITLE OF THESIS/*TITRE DE LA THÈSE* Intercalation of Silver in titanium disulphide.

UNIVERSITY/*UNIVERSITÉ* SIMON FRASER UNIVERSITY

DEGREE FOR WHICH THESIS WAS PRESENTED/*GRADE POUR LEQUEL CETTE THÈSE FUT PRÉSENTÉE* M. Sc.

YEAR THIS DEGREE CONFERRED/*ANNÉE D'OBTENTION DE CE GRADE* 1982

NAME OF SUPERVISOR/*NOM DU DIRECTEUR DE THÈSE* PROF. R. FRINDT

Permission is hereby granted to the NATIONAL LIBRARY OF CANADA to microfilm this thesis and to lend or sell copies of the film.

The author reserves other publication rights, and neither the thesis nor extensive extracts from it may be printed or otherwise reproduced without the author's written permission.

L'autorisation est, par la présente, accordée à la BIBLIOTHÈQUE NATIONALE DU CANADA de microfilmer cette thèse et de prêter ou de vendre des exemplaires du film.

L'auteur se réserve les autres droits de publication; ni la thèse ni de longs extraits de celle-ci ne doivent être imprimés ou autrement reproduits sans l'autorisation écrite de l'auteur.

DATED/*DATÉ* 16 Dec '82 SIGNED/*SIGNÉ*

PERMANENT ADDRESS/*RÉSIDENCE FIXÉ*

[redacted]

NL-91 (3-74)

INTERCALATION OF SILVER IN TITANIUM DISULPHIDE

by

D.K.Kaluarachchi
B.Sc.(Hon.), University of Sri Lanka, Vidyodaya Campus, 1977

THESIS SUBMITTED IN PARTIAL FULFILLMENT OF
THE REQUIREMENTS FOR THE DEGREE OF
MASTER OF SCIENCE
in the Department
of
Physics

SIMON FRASER UNIVERSITY

SEPTEMBER, 1982

APPROVAL

Name: Dayakanthi Kaluarachchi

Degree: Master of Science

Title of Thesis: Intercalation of Silver in Titanium Disulphide

Examining Committee:

Chairperson: B. P. Clayman

R. F. Frindt
Senior Supervisor

A. E. Curzon

D. J. Huntley

S. R. Morrison
External Examiner
Professor
Department of Physics
Simon Fraser University.

Date Approved: October 13, 1982

PARTIAL COPYRIGHT LICENSE

I hereby grant to Simon Fraser University the right to lend my thesis, project or extended essay (the title of which is shown below) to users of the Simon Fraser University Library, and to make partial or single copies only for such users or in response to a request from the library of any other university, or other educational institution, on its own behalf or for one of its users. I further agree that permission for multiple copying of this work for scholarly purposes may be granted by me or the Dean of Graduate Studies. It is understood that copying or publication of this work for financial gain shall not be allowed without my written permission.

Title of Thesis/~~Project/Extended Essay~~

Intercalation of Silver in titanium disulphide.

Author:

(signature)

DAYAKANTHI KALUARACHCHI
(name) (Last name)

16th Dec '82
(date)

ABSTRACT

The motion of stage 1 and stage 2 silver in partially intercalated TiS_2 crystals was studied by determining the relative amount of silver in TiS_2 crystals as a function of position, using a scanning electron microscope with an x-ray fluorescence attachment. The stage 1 silver converted rapidly into stage 2 silver at room temperature. The stage 2 front remained stationary for long periods at room temperature and silver was observed to migrate throughout the TiS_2 crystal at elevated temperatures.

Radioactive tracer experiments showed that when silver atoms enter a partially intercalated stage 2 TiS_2 crystal most of the newly intercalated guest atoms reside near the crystal edge. Additionally it was found that when the conversion of stage 1 to stage 2 occurred, most of the stage 1 silver remained near the crystal edge after converting into stage 2. The stage 1 to stage 2 conversion can be explained by Daumas and Herold's model while the classical model fails to do so. An island size of about 130 Å was obtained for the stage 2 region using the x-ray fluorescence data. The motion of silver perpendicular to the layers in the TiS_2 lattice was not observed at room temperature ($D < 10^{-15}$ cm^2/sec) and the estimated diffusion coefficient at 200 °C was $\sim 10^{-13}$ cm^2/sec.

ACKNOWLEDGEMENTS

I wish to express my deepest gratitude to my supervisor Dr.R.F.Frindt, for his invaluable guidance, encouragement and patience through out the entire period of this research work.

My special thanks are due to Per Joensen for his willing assistance and valuable advice on experiments and for help kindly given me in many ways during the period of this research.

Many thanks are due to the members of the examining committee, Dr.A.E.Curzon and Dr.D.J.Huntley for reading the manuscript within a short period and for their helpful suggestions.

I am very grateful to Dr.J.M.D'Auria of the Department of Chemistry of S.F.U. for valuable discussions and assistance given me for the experiments in chapter 4. Also, I would like to thank the Department of Chemistry, S.F.U. for allowing me to use their radiochemistry laboratory for the experiments in chapter 4.

I am grateful to the Department of Biology, S.F.U. for allowing me to use their scanning electron microscope very frequently. Many thanks are due to Dr.V.Bourne of the Department of Biology, S.F.U. for the skillful help given me in operating the SEM. I also wish to thank Dr.K.Colbow of the Physics Department and his research group (especially Sara Swenson) for allowing me to use their interference microscope often.

The financial assistance from my supervisor Dr.R.F.Frindt through a research grant from the Natural Sciences and Engineering Research Council of Canada along with the President's Research grant and the teaching assistantships from S.F.U. are also very gratefully acknowledged.

Many thanks are due to Ranjith Divigalpitiya who helped me to type this thesis. I am grateful to the Instructional Media Centre of S.F.U. for

the useful suggestions and willing help given me for the graphical work.

My thanks are due to the faculty, the technical staff (especially Siva Chinniah), the secretarial staff and all the other members of the Physics Department for their help and friendly cooperation.

At last, but not least, I am very much thankful to my dear parents and to the University of Sri Jayawardenepura, Sri Lanka who made it possible for me to come to the Simon Fraser University.

TABLE OF CONTENTS

LIST OF TABLES

LIST OF FIGURES

I. Introduction

1.1. Transition metal dichalcogenides

The transition metal dichalcogenides have received considerable attention in recent years because these materials are potential candidates for cathodes in electrointercalation batteries(1). The layered transition metal dichalcogenides (MX_2) are formed by combining the transition metals(M) of groups IV to VI of the periodic table with the chalcogens(X), S,Se, and Te. These compounds consist of strongly bonded X-M-X sandwiches which are stacked upon each other and held together with weak bonds. Fig.1.1 shows the general form of these layer structures. This basic atomic structure makes these materials extremely anisotropic in their physical properties.

The coordination unit for the MX_2 stucture is found to take either the trigonal prismatic or the octahedral form as shown in Fig.1.2. The crystal unit cell consists of one or more than one layer depending on the particular compound. A full review and details of these compounds are found in references (2) and (3).

1.2. Intercalation

Intercalation refers to the insertion of guest species in between the layers of a host structure. In transition metal dichalcogenides, the intralayer bonding is strong and covalent while the interlayer bonding is of the Van der Waals type. This weak bonding between the layers permits the opening up of the layers and the entry of the guest species. Many metals, hydrogen, ammonia and organic molecules have been intercalated into

the layer compounds. In fact it is generally observed that any species that is an electron donor can be intercalated into the layer compounds, and there is evidence that there is a transfer of negative charge ("charge donation") from the intercalated metal to the host layers(4). Insertion of atoms is generally accompanied by a small reversible expansion of the host lattice in the direction of c axis, typically 5 to 10 percent. The host layer 'a' spacing generally increases by only one percent (5). The intercalated atoms reside in sites in the Van der Waals gaps which are either octahedral, tetrahedral or trigonal prismatic, depending on the stacking of the host layers. On deintercalation the host lattice generally returns to its original structure (4).

The intercalation of metals is usually accomplished either by electrointercalation or by intercalation from a vapor at elevated temperatures. In the experiments which will be discussed in this thesis the electrointercalation technique was used.

1.3. Staging and the models of staging

The structure determination of the intercalated compounds has shown that intercalation generally occurs in "stages" (6). The stage of a compound is defined as the ratio of the number of host layers to the number of guest layers. When all the gaps between host layers are occupied by an intercalated layer, the compound is said to be "first stage". In a "second stage" compound every other layer of the host lattice is on average occupied by intercalated atoms. In the same way one can define higher stages of a compound. Some theoretical studies have attempted to explain the process of staging considering the coulomb interaction between intercalated ions and the strain effects in the host lattice (7,8,9), however the process of staging is not yet particularly well understood.

1.3.1. The classical model of staging

The classical model for the arrangement of guest atoms in the host lattice of different stages is shown in Fig.1.3. In this model, some layers of the host crystal are entirely occupied and some layers are completely empty. This model has difficulty in explaining the formation of higher stages by a rearrangement of the guest atoms in the layers of the host lattice. For example, suppose a compound of third stage is formed from second stage. A compound of second stage would correspond to the occupation of gaps 1,3,5,7,9,11,..etc (Fig.1.3). A third stage compound would correspond to the occupation of gaps 1,4,7,10,13,16,...etc. Therefore the formation of a compound of third stage from second stage supposes the evacuation of all gaps 3,5,9,11...etc and the filling of all gaps 4,10,16,20,...etc, a process which seems to be rather improbable.

1.3.2. Daumas and Herold s model of staging: the island model

To explain the rearrangements required for stage conversion in a crystal, Daumas and Herold (10) proposed a model which avoids the topological problems associated with the classical model. A schematic diagram for Daumas and Herold's model is shown in Fig.1.4. In this model the guest atoms are found in all the layers of the host lattice but the layers are only partially filled and islands of guest atoms are arranged in a manner to form the different stages. In this model for a certain stage the sequence of host and intercalated layers in the 'c' direction is the same as for the classical model.

Daumas and Herold's model provides a convenient interpretation for various reaction mechanisms. The passage from stage 1 to stage 2 or any other higher stages can be simply explained by an appropiate regrouping of

the guest atoms within a layer than a total evacuation of some gaps. In fact in Daumas and Herold's Model, (for a constant amount of intercalant in the crystal) the total amount of intercalant in a given layer remains constant in any stage conversion.

Daumas and Herold's model has not undergone convincing verification. In this thesis some experimental results will be presented in chapter 5 in support of the Daumas and Herold's model.

1.4. Crystal structure of TiS_2 and $Ag_x TiS_2$

Titanium disulphide is not a naturally occuring compound. Single crystals of TiS_2 can be prepared by the iodine vapour transport technique (11,12,13) yielding plate-like crystals typically 10 to 100 μm thick and 2 to 5 millimeters wide. TiS_2 crystals are golden in colour and the specific gravity is 3.22. Electrically, TiS_2 has semimetallic properties (3).

The TiS_2 crystal structure consists of loosely coupled S-Ti-S atom sheet sandwiches as shown in Fig. 1.1, where X = S and M = Ti. Each sandwich is made of a close-packed layer of titanium atoms between two close-packed layers of sulphur atoms. TiS_2 has the cadmium iodide structure shown in Fig. 1.5 (14,15). The TiS_2 referred to here is commonly written as 1T-TiS_2 where the 1T indicates that there is a one layer stacking sequence and that the primitive unit cell is trigonal.

The structure of $Ag_{0.2} TiS_2$ and $Ag_{0.4} TiS_2$ have been recently determined(16). The value of 0.4 for the mole fraction of Ag in TiS_2 is of particularly interest because it is the maximum value that is obtained when Ag is electrochemically intercalated into TiS_2 (16). Only stage 1 and stage 2 have been observed for $Ag_x TiS_2$ and the mole fractions 0.4 and 0.2 correspond to stage 1 and stage 2 respectively(16). In both $Ag_{0.2} TiS_2$ and $Ag_{0.4} TiS_2$, Ag is located in octahedral sites in the Van der Waals gap. In

the Van der Waals gaps there are one octahedral site and two tetrahedral sites per Ti atom. The unit cells and the lattice constants for $Ag_{0.2}TiS_2$ and $Ag_{0.4}TiS_2$ are given in Fig. 1.6.

1.5. Diffusion in solids and in intercalation compounds

1.5.1. Diffusion in solids

Diffusion is a process by which matter is transported from one part of a system to another as a result of random atomic motions. The difference in concentration of atoms in a solid leads to a flux of these atoms through the solid until equilization of concentration is obtained. For simple diffusion the number of atoms of one species passing per unit time perpendicularly through a reference surface of unit area is proportional to the concentration gradient of the same species measured normal to the reference surface, and is given by, Fick's law,

$$J = - D \frac{\partial c}{\partial x}$$

where,

J = net number of atoms crossing unit area in unit time,

c = the concentration of the diffusing atoms,

x = the space coordinate chosen perpendicular to the reference surface and

D = the diffusion coefficient (also called the diffusivity).

The minus sign indicates that the diffusion occurs away from the region of high concentration.

The diffusion coefficient increases with temperature according to the relation,

$$D = D_o \exp (-E/k_B T)$$

where,

E = activation energy for the process,

T = absolute temperature and

k_B = Boltzmann's constant.

To move an atom through interstitial sites in a lattice, the atom must surmount the potential energy barrier created by its neighboring atoms. The atoms with sufficiently high thermal energy can pass over the energy barrier. The probability p, for an atom to jump over the energy barrier is given by (17),

$$p = \nu \exp (-E/k_B T)$$

where,

ν = characteristic atomic vibrational frequency,

E = height of the energy barrier or the activation energy for the process.

p is often called the jump frequency.

When the diffusion occurs between two sites separated by a distance 'a', the diffusion coefficient can be written as,

$$D = \nu a^2 \exp (-E/k_B T)$$

If the diffusing atoms are charged the ionic mobility (μ) can be found from the diffusivity by using the Einstein relation $k_B T\mu = qD$. Then the ionic mobility is given by,

$$\mu = \frac{q\nu a^2}{k_B T} \exp (-E/k_B T)$$

where,

q = charge of the mobile ion.

1.5.2. Diffusion in intercalated compounds

High diffusivity of guest ions through layered structures is desired for fast discharge rates in intercalation batteries(1) and a high alkali ion diffusivity in the Van der Waals gaps of various layered compounds has been reported(1,4). Since the guest atoms most likely reside in the sites in the Van der Waals gaps as positively charged ions (1,4) the electrostatic repulsive forces tend to keep them apart. As a result the height of the energy barrier will be decreased relative to the situation for uncharged atoms resulting in an increase of diffusivity of ions in the lattice.

Since Ag ions reside in octahedral sites in the Van der Waals gaps of the TiS_2 crystals the diffusion in Ag ions involve jumps between the octahedral sites via a tetrahedral site (Fig.1.7 (a)). Since the tetrahedral sites are smaller than the octahedral sites (4), the expected energy profile for the mobile ions in TiS is expected to be similar to that shown in Fig.1.7 (b).

Some factors that may affect the diffusion of guest atoms in the Van der Waals gap are mentioned in reference (4). For example, the increase in c lattice parameter on intercalation increases the size of the octahedral and tetrahedral sites through which the ions move, but it is not clear that this increase in the size of the sites will result in an increase in the mobility of the guest atoms in the host lattice. This is because the degree of ionization of the guest atoms may decrease with the increase in the guest ion content (4) in the host lattice which may increase the effective ionic size of guest atoms. As a result the relative size of the

guest ion to site may not be changed significantly. In a lattice with high ionicity the potential variation that the guest ion sees will be greater than in a more covalent lattice. Therefore the ionicity of the lattice is expected to lower the mobility of ions. The degree of filling of the lattice may also govern the diffusion: if the number of available empty sites around the guest ions is large, the probability of an ion jumping into a new site is also higher. Diffusion may be hindered in a nonstochiometric lattice with excess amount of transistion metal, where the excess metal probably occupies the sites available for guest atoms.

1.6 Contributions of this thesis

Although alkali metals such as Li and Na are the most interesting guest species for intercalation batteries because of their high mobility and high free energy of formation (1,4), from an experimental viewpoint the high reactivity and the need for water-free electrolytes makes it very inconvenient to use alkali metals in many experiments. In addition, the X-ray fluorescence technique is not suited to the observation of intercalants with atomic weights as low as Li and Na. Therefore pseudo-alkali metals such as silver and copper have been used in much intercalation research work.

In this thesis an investigation of the motion and distribution of silver (guest) in titanium disulphide (host) is presented. The distribution of the intercalant (silver) is studied by determining the silver (Ag) concentration as a function of position in the titanium disulphide (TiS_2) crystal. In some experiments presented, a scanning electron microscope with an X-ray fluorescence attachment was used to determine the silver distribution. In other experiments, radioactive and nonradioactive silver were used as the intercalant and the crystal activity was measured to

determine the Ag distribution in the crystal.

Chapter 2 gives a brief introduction to the scanning electron microscope and the X-ray fluorescence technique (XRF).

In chapter 3 a study of motion of both stage 1 and stage 2 silver in the TiS_2 is discussed. Some experiments were done at elevated temperatures. This study is only concerned with the motion within the Van der Waals layers.

A radioactive tracer experiment, presented in chapter 4, was done to investigate the migration of Ag atoms in TiS_2 . Stage 2 silver was studied to observe the motion of silver while the crystal was being intercalated and the motion of stage 1 silver was studied after intercalation ceased.

In chapter 5 the order of magnitude of the stage 2 silver island width is estimated assuming the island model configuration and using XRF data obtained in chapter 3.

A study of the motion of Ag along the c axis of the TiS_2 lattice is described in chapter 6. A discussion is given at the end of each chapter and the conclusion is given in chapter 7.

Fig. 1.1. The sandwich structure of MX_2 compounds (cross section)

X - chalcogen
M - transition metal

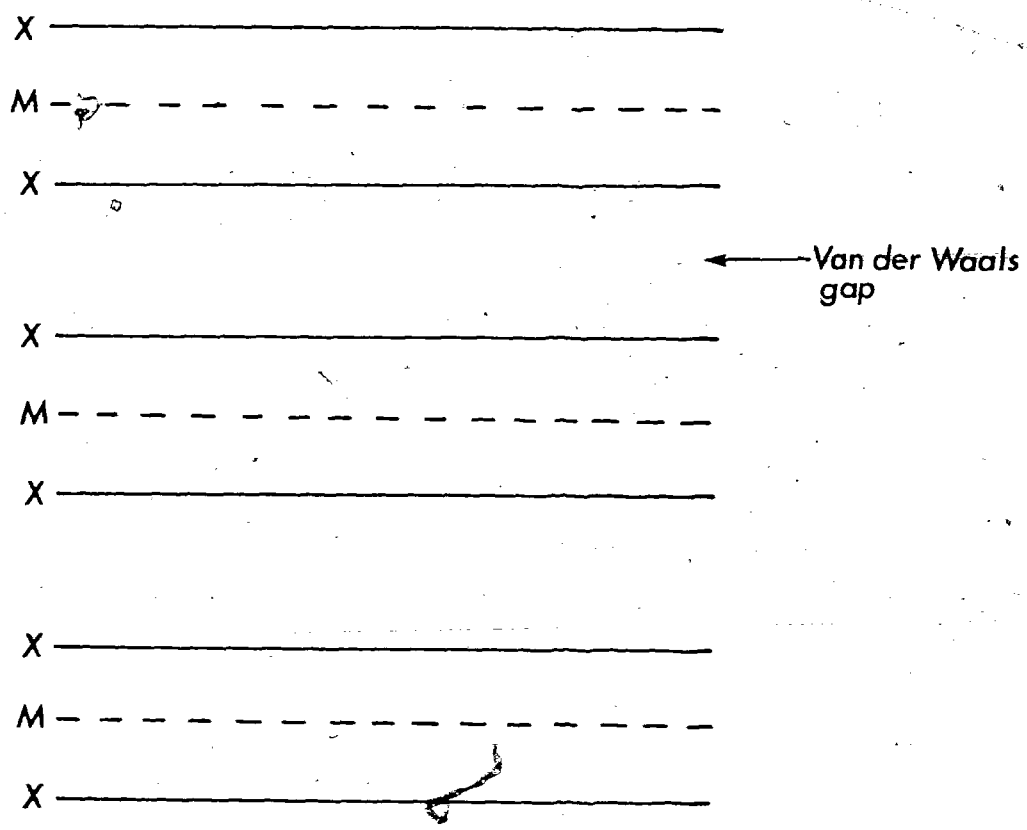

Fig.1.1

Fig. 1.2. The coordination around the metal ions
(a) Octahedral structure
(b) Trigonal prismatic structure

● - transition metal
○ - chalcogen

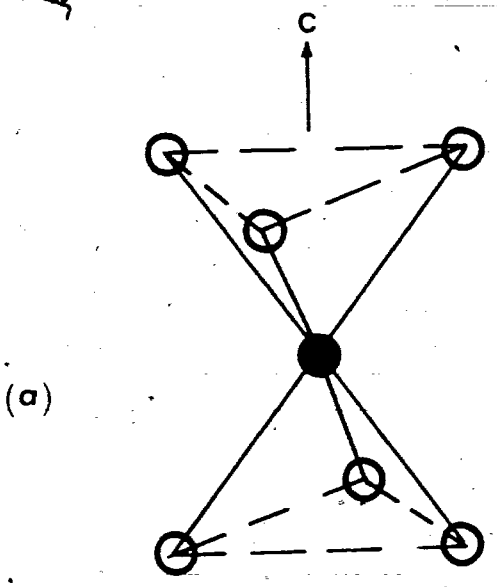

(a)

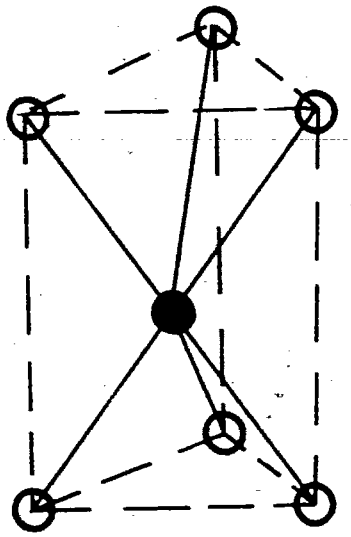

(b)

Fig. 1.2

Fig. 1.3. Different stages in the classical model of staging

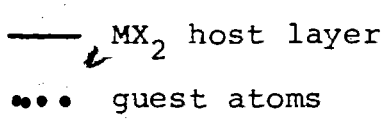

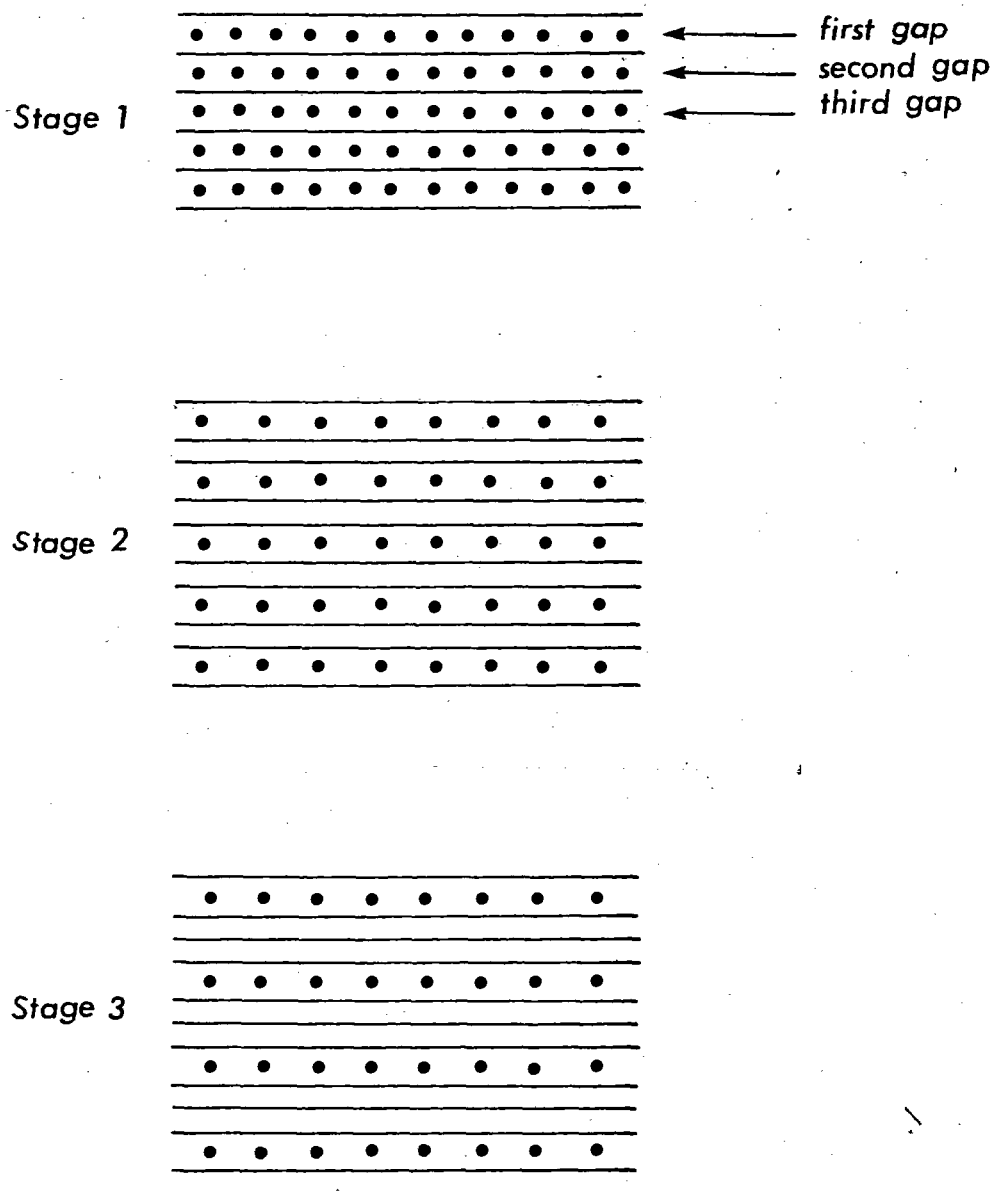

Fig.1.3

Fig. 1.4. Daumas and Herold's model of staging

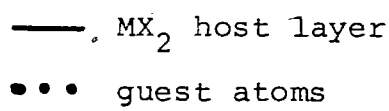

Stage 1

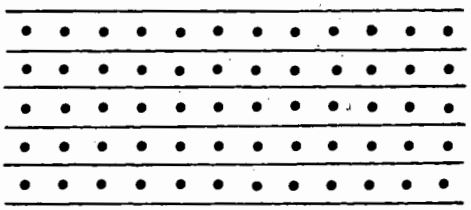

Stage 2

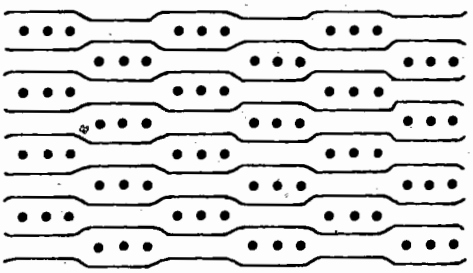

Stage 3

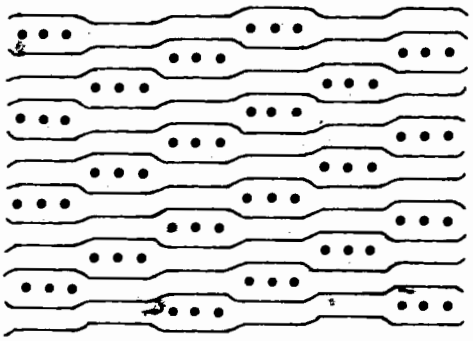

Fig. 1.4

Fig. 1.5. (a) The atomic structure of TiS_2.
The prefix 1T refers to the 1 layer unit-cell with trigonal(T) symmetry.

(b) The $(11\bar{2}0)$ diagonal cross section of the TiS_2 unit cell (from ref. 16)

Fig. 1.6. The $(11\bar{2}0)$ diagonal cross section of the unit cells of $Ag_{0.4}TiS_2$ and $Ag_{0.2}TiS_2$.

(a) $Ag_{0.4}TiS_2$

(b) $Ag_{0.2}TiS_2$ (from ref. 16)

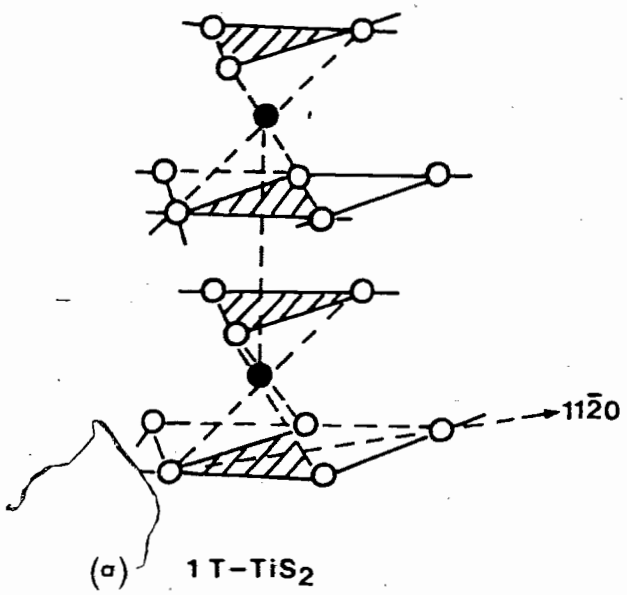
$11\bar{2}0$
(a) 1 T–TiS_2

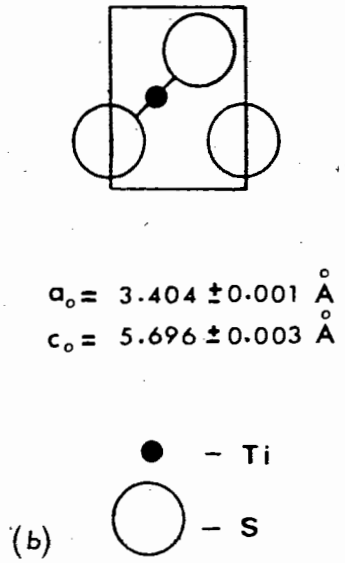
a_o = 3.404 ± 0.001 Å
c_o = 5.696 ± 0.003 Å
– Ti
– S
(b)

Fig. 1.5

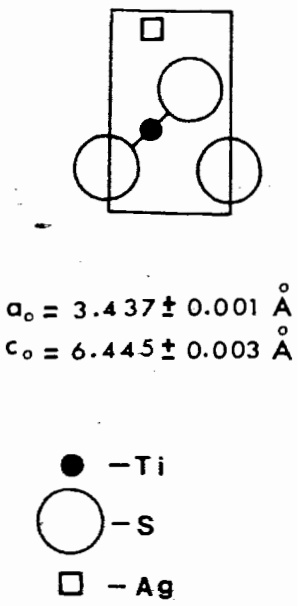
a_o = 3.437 ± 0.001 Å
c_o = 6.445 ± 0.003 Å
– Ti
– S
– Ag
(a)

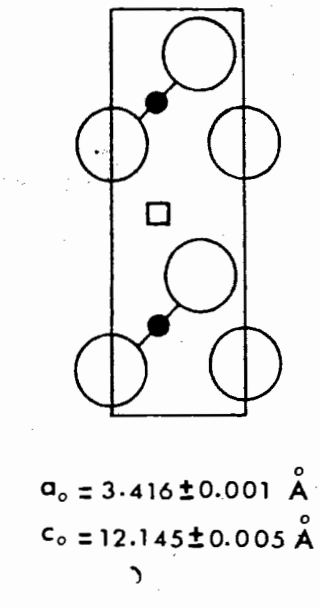
a_o = 3.416 ± 0.001 Å
c_o = 12.145 ± 0.005 Å
(b)

Fig. 1.6

Fig. 1.7. (a) The zig-zag line shows the path of an ion from octahedral ⟶ tetrahedral ⟶ octahedral sites(3).

(b) Expected energy profile of mobile ions(3).

(a)

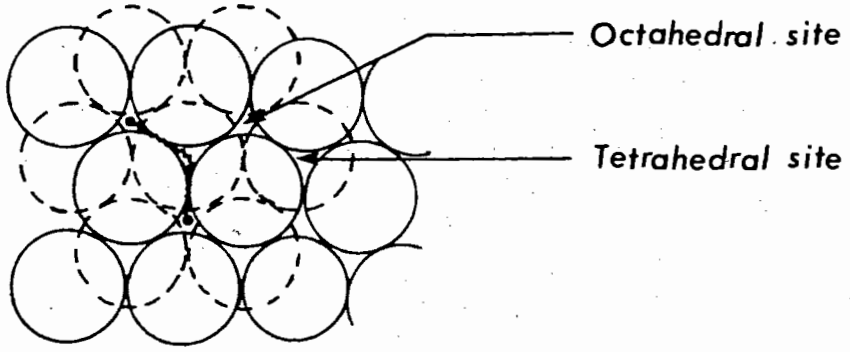

S atoms on the plane of figure

S atoms out of the plane

guest atoms

(b)

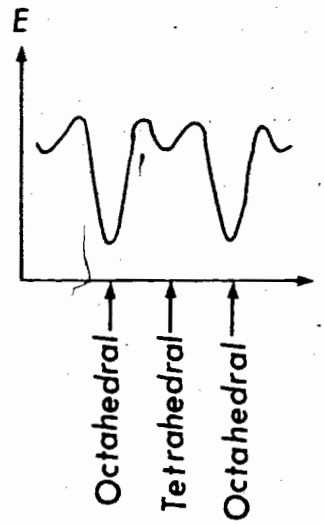

Fig. 1.7

II. The electron microscope and x-ray fluorescence

2.1 The scanning electron microscope.

The scanning electron microscope (SEM) is a powerful instrument for the examination and analysis of solids on a micrometer scale. The primary reason for the SEM's usefulness is the high resolution which is typically in the range 50 to 200 Å. Another important feature of the SEM is the three dimensional appearance of the images. Attachments such as x-ray fluorescence (XRF) make the SEM specially useful for solid state studies.

The basic components of the SEM are the electron gun, lens system, electron collector, visual and recording cathode ray tubes and the electronics associated with them (Fig.2.1). In the electron gun, thermionically emitted electrons are accelerated by potentials of up to 30 to 40 kV. The condenser and the objective lens systems are used to demagnify the electron beam to the final spot size on the sample. These lenses are generally electromagnetic lenses and the shape and the strength of the magnetic field determine the focal length of the lens.

The area to be examined is irradiated with a finely focussed electron beam, which is swept in a raster across the surface of the specimen. When the electron beam impinges on the specimen surface different types of signals are emitted including characteristic x-rays, secondary electrons and back scattered electrons of various energies. These signals are used to measure characteristics of the specimen such as composition, surface topography, crystallography, etc. A detailed description of the electron microscope is given in reference (18).

In experiments discussed in this thesis an ETEC model Autoscan Scanning Electron Microscope was used. In this microscope a maximum resolution of about 150 Å can be obtained at an accelerating voltage 30 kV. The accelerating potential can be selected to have any of the values 2.5, 5, 10, 20 and 30 kV. In our experiments, an area of about 2 square micrometers of the specimen surface was scanned at a time and the voltages of either 10 kV or 20 kV were used.

The spatial configuration of the electron beam inside a specimen from the centre of impact depends on the electron beam energy and the elements in the specimen. This is schematically indicated in Fig.2.2.

2.2 X-ray fluorescence spectra

X-ray fluorescence spectrometry is a very useful method for chemical analysis of many different types of samples. When a sample is bombarded by sufficiently energetic electrons, x-rays are emitted as noncharacteristic continuous spectra and as line or band spectra having wave lengths characteristic of the emitting element. X-ray fluorescence (XRF) spectra are produced by secondary fluorescence when characteristic x-rays or continuous x-rays interact with the inner shell electrons of the atoms in the sample. Radiation of sufficiently high energy can remove an inner shell electron of an atom leaving the atom in an excited state. Then the atom returns to a stable state by the transition of an outer electron into the vacancy in the inner shell, emitting an x-ray photon. The energy of fluorescent x-rays identifies the emitting element, and the intensity is related to the weight concentration of the element within the analysed volume. The spatial configuration for fluorescent x-rays is shown in Fig.2.2 (b). A detailed description of x-ray spectrometry analysis is given in (19).

In our experiments an energy dispersive x-ray detector (Si/Li detector system) attached to the SEM was used to detect the XRF spectra. The x-ray signal from the sample is passed through the high resolution ($\triangle E \sim 150$ eV) solid state detector (Si/Li) and the amplified output signal which is proportional to the x-ray energy was passed to a multichannel analyzer. In the multichannel analyzer electronic pulses are sorted so that the final output gives the intensity of x-rays as a function of energy.

With XRF spectra a sample can be anlyzed either qualitatively or quantitatively. For a quantitative analysis the relative x-ray intensities of the specimen to a standard are measured in order to cancel out uncertain terms, such as the absolute detector efficiency and instrumental drift. To obtain an absolute concentration for an element in the sample, the measured intensity ratio for that element should be adjusted by several other corrections such as background, atomic number and absorption (20).

For the experiments in this thesis our main interest was to find the relative distribition of silver in TiS crystals as a function of position. Since the absolute concentration of silver in the sample was not required the correction factors mentioned above were not necessary. The data obtained were corrected for the background and the ratio of the x-ray intensities of Ag to Ti was measured to avoid the errors due to instrumental drift.

2.3 X-ray fluorescence spectra from $Ag_x TiS_2$

Typical XRF spectra for $Ag_{0.4}TiS_2$, $Ag_{0.2}TiS_2$ and TiS_2 are shown in Fig.2.3. The spectra were obtained at 20 kV and peaks correspond to the S K_α line at 2.308 keV, the Ag L_α line at 2.984 keV and Ti K_α line at 4.510 keV. The area under a peak is related to the abundance of the corresponding element in the sample. In our experiments the x-ray

intensities for the Ag L_{α} and Ti K_{α} peaks were measured using a window of width 0.30 keV as indicated in Fig.2.3.

2.4 The depth of origin of detectable fluorescent x-rays in pure TiS_2 at 10 kV and 20 kV

When studying a specific system, it is important to know the maximum depth of origin of detectable fluorescent x-rays. An experiment was done to find this depth in pure TiS_2. Obviously the depth of origin of fluorescent x-rays depends on the penetration depth of the electron beam (or the incident energy of the electron beam).

A thin layer of Ag was evaporated onto pieces of cover glass and on each of them a small area was scratched off. Thin TiS_2 crystals with thicknesses ranging from 0.5 to 2.5 μm were prepared (section 3.2, chapter 3) and mounted on the silver evaporated cover glass pieces so that, a part of the crystal was in contact with the silver layer and the other part of the crystal was lying on bare glass. XRF spectra from different regions of the crystal were obtained. If the electron beam penetrated through the crystal a peak for silver was observed in XRF spectrum from the crystal region lying on the deposited layer of silver. A peak for silver was of course not observed in the XRF spectrum from the region lying on bare glass.

It was found that when a crystal of thickness 1.2 μm was examined with a 10 kV electron beam, the fluorescent x-ray peak obtained from silver was weak, and no silver peak was observed when a 1.5 μm thick crystal was used. Similarly at 20 kV, a weak peak from the silver was obtained when the crystal thickness was 1.8 μm and for a crystal of thickness 2 μm the fluorescent x-rays from the silver was not observed.

Therefore in pure TiS_2 the maximum depth of the origin of the detectable fluorescent x-rays is in between 1.2 and 1.5 μm at 10 kV and it is in between 1.8 and 2 μm at 20 kV. For Ag_xTiS_2 this depth is expected to be less due to a reduced penetration of the electron beam and increased x-ray absorption.

Fig. 2.1. Basic components of the scanning electron microscope with x-ray fluorescence attachment.

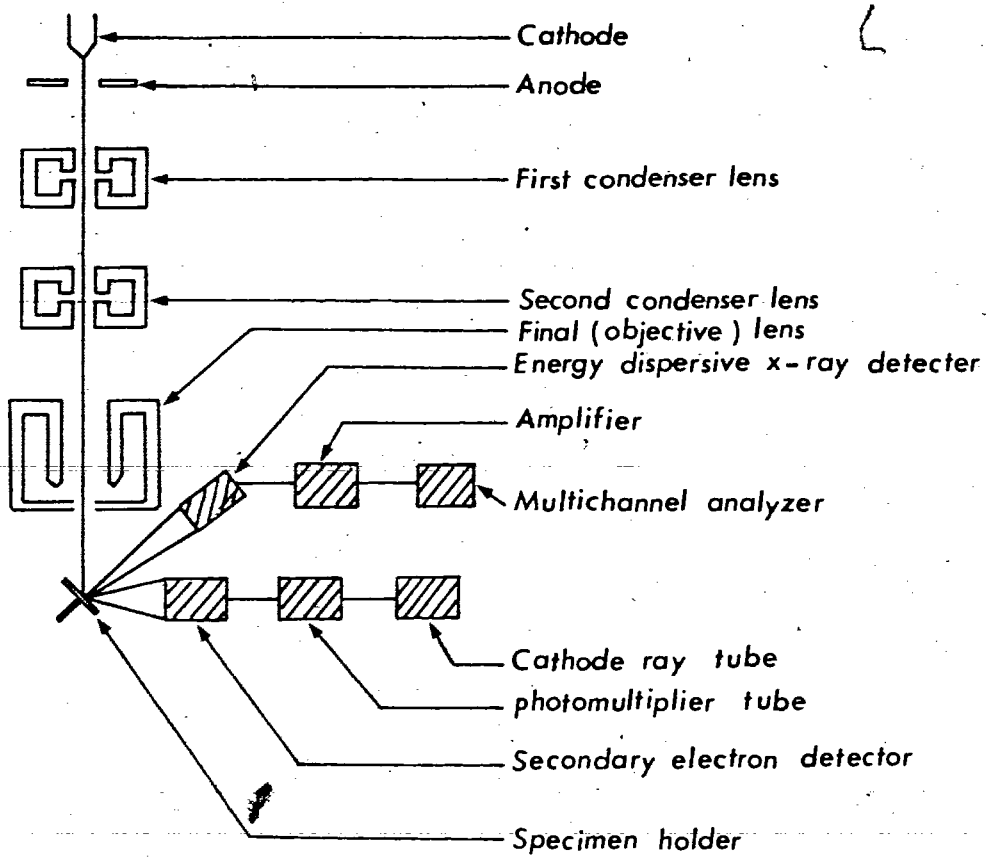
Cathode
Anode
First condenser lens
Second condenser lens
Final (objective) lens
Energy dispersive x-ray detecter
Amplifier
Multichannel analyzer
Cathode ray tube
photomultiplier tube
Secondary electron detector
Specimen holder

Fig. 2.1

Fig. 2.2. (a) The variation of electron scattering with voltage and atomic number(13).

(b) Diagram indicating the typical spatial distribution for electrons and x-rays within the sample(13).

The scale,within the sample depends on the sample elements and the incident electron beam energy.

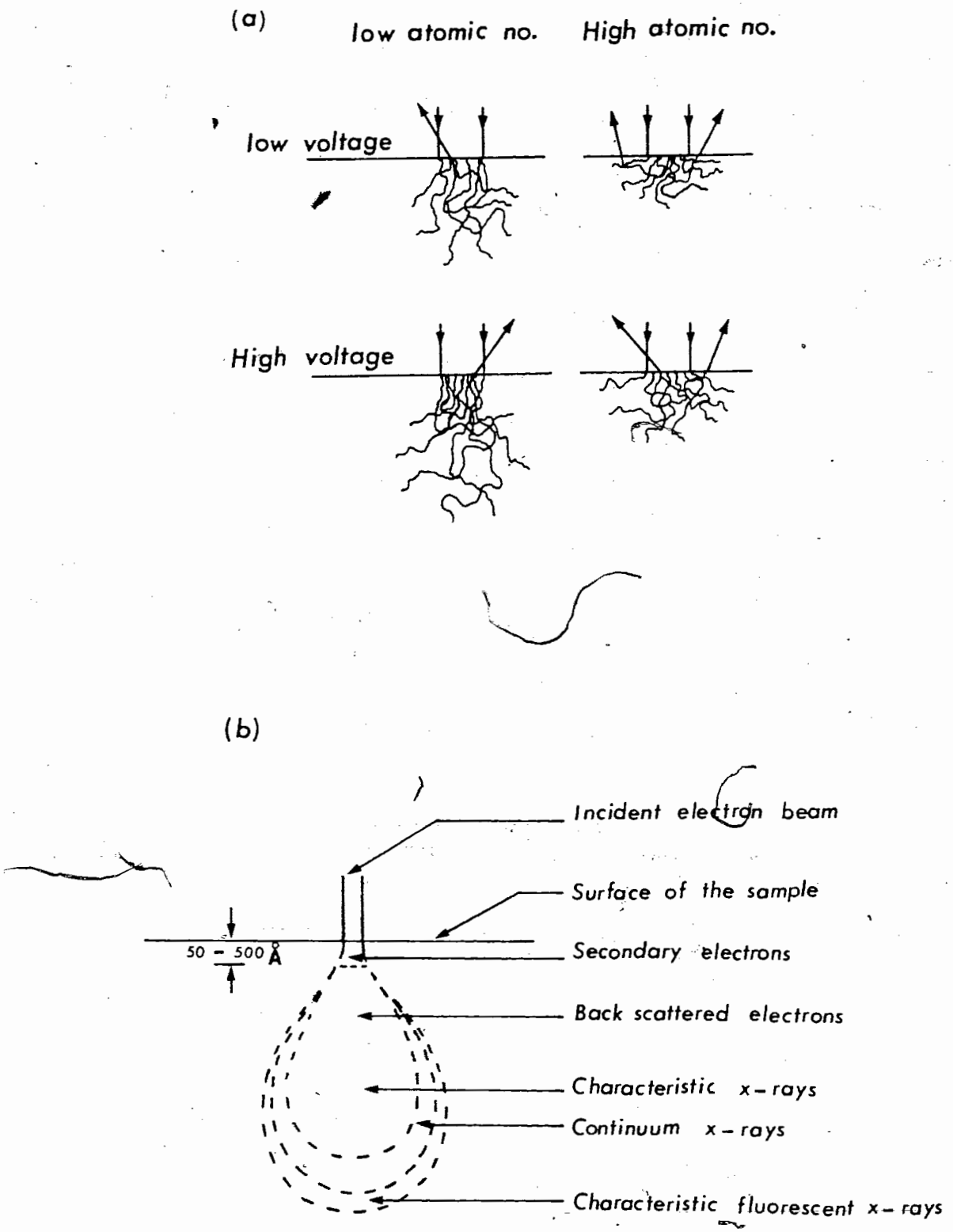
(a)
low atomic no.
High atomic no.
low voltage
High voltage
(b)
Incident electron beam
Surface of the sample
50 - 500 Å
Secondary electrons
Back scattered electrons
Characteristic x-rays
Continuum x-rays
Characteristic fluorescent x-rays

Fig. 2.2

Fig. 2.3. Typical x-ray fluorescence spectra for

(a) $Ag_{0.4}TiS_2$

(b) $Ag_{0.2}TiS_2$

(c) TiS_2

These data were taken by P. Joenson.

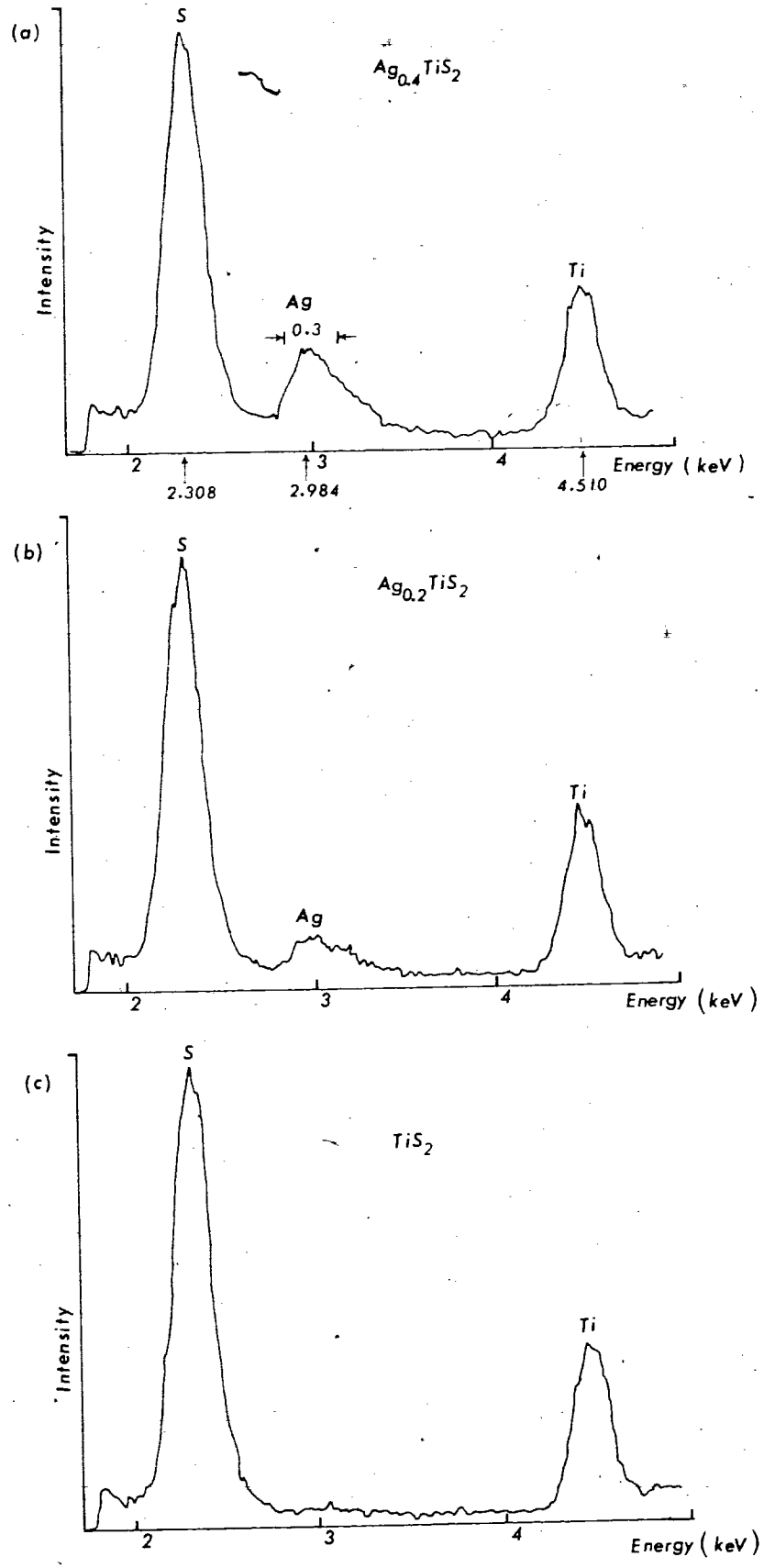
(a)
S
$Ag_{0.4}TiS_2$
Intensity
Ag
0.3
Ti
2
3
4
Energy (keV)
2.308
2.984
4.510
(b)
S
$Ag_{0.2}TiS_2$
Intensity
Ti
Ag
2
3
4
Energy (keV)
(c)
S
TiS_2
Intensity
Ti
2
3
4
Energy (keV)

Fig. 2.3

III. Study of stage 1 and stage 2 silver in TiS_2 using the scanning electron microscope and x-ray fluorescence

3.1 Introduction

The intercalation of silver into crystals in an electrolyte of 0.1 M solution of $AgNO_3$ in water or glycerol occurs in two stages (21). In a partially intercalated TiS_2 crystal there are three distinct regions namely, stage 1, stage 2 and empty crystal (Fig.3.1 (a) and (b)). The region near the edge of the crystal is stage 1 and it has an atomic composition of x = 0.42 +/- 0.02 (16) which tends to be constant as the crystal intercalates. Further in from the edge, and next to stage 1 a stage 2 region is found where the x value drops to half of the stage 1 value. Beyond the stage 2 region the crystal is empty of silver and x = 0. These stages can be observed optically in either transmission or reflection. The optical reflection decreases when the crystal is intercalated and the stage 1 region appears darker or less reflecting than the stage 2 region, and the stage 2 region appears darker than the empty crystal. Conversely, the use of transmitted light for thin transparent crystals shows the opposite observation (21). The position of the fronts observed in reflection are readily identified (Fig.3.1 (b)) and this work shows that the fronts have the same locations as those observed using XRF microprobe for crystals in the 1 to 2 μm range.

In this chapter a study of the distribution (or motion) of the stage 1 and stage 2 phases of silver in partially intercalated TiS_2 crystals is presented. The relative amount of silver in the crystal was determined as a function of position using a scanning electron microscope and x-ray

fluorescence attachment. The work includes a study of motion of both stage 1 and stage 2 silver in TiS_2 at room temperature and also the motion of stage 2 silver at elevated temperatures.

3.2 Sample preparation and intercalation

3.2.1 Sample preparation

The thickness of TiS_2 crystals that were used in the experiments were in the range 1 to 2 μm. The lateral dimensions of the crystals were usually less than 1000 μm. The pure TiS_2 crystals were prepared by the "iodine vapor transport" method and were typically more than 10 μm, so that the crystals used for intercalation were obtained by cleaving the as-grown crystals.

To cleave TiS_2 crystals to micrometer thicknesses a thin layer of epoxy was spread onto a microscope slide and a few as-grown crystals were laid flat on the epoxy. Thin cystals were peeled from the thick crystals using sticky tape. The peeled thin crystals were removed from the tape by dissolving the glue on the tape in trichloroethylene. Using fine forceps or an eye dropper the crystals were removed from the trichloroethylene and placed on a piece of microscope cover glass. The thicknesses of the crystals were determined to an accuracy of +/- 0.07 μm using a Wild M 20 microscope with an interference attachment. The steps used in sample preparation are shown in Fig.3.2. A graphite block was fixed with some graphite dag to a SEM sample holder and the piece of cover glass with the crystal was placed on top of the graphite block (Fig.3.2 (a), (b), (c)). The graphite block was used to keep the SEM sample holder away from the electrolyte because otherwise the aluminium of the sample holder might have

intercalated into the crystal. Also, the graphite block eliminated XRF peaks from the aluminium and impurities in the sample holder. Next the corners of the cover glass and the crystal were glued down with some RTV silicone rubber (Fig.3.2 (d)). A narrow layer of graphite dag was applied from a side of the crystal to the graphite block to make electrical contact between the crystal and the sample holder. (The graphite dag (Electrodag 154 from Acheson Colloids, Ontario) used in these experiments is high purity fine graphite particles in suspension in isopropyl alcohol.) The graphite layer was then covered with RTV silicone rubber to prevent it from being washed away by the electrolyte (Fig.3.2 (e)). The crystals were allowed to intercalate only from one edge by covering the other edges with RTV. Finally, all the RTV and glass were covered with graphite dag since nonconducting materials tend to charge up when they are exposed to the electron beam of the SEM. The sample preparation from Fig.3.2 (d) to (f) was done under a low power optical microscope.

3.2.2 Intercalation of TiS_2 with silver

A 0.1 M solution of $AgNO_3$ in glycerol was used as the electrolyte. It was found that when water was used as the solvent, a considerable amount of cracking occurs at the crystal edge whereas with glycerol the intercalation rate was slower and only a few or no cracks in the crystals were observed. The samples were intercalated electrochemically as shown in Fig.3.3. The microscope slide with the sample and the electrolyte were placed on an optical microscope, so that the process of intercalation could be observed. Since the intercalation rate is thickness dependent (21), the period of intercalation varies from crystal to crystal. The crystals which were used in this experiment were usually intercalated for about 4 to 5 hrs resulting in a partially intercalated crystal as shown in Fig.3.1 (b).

The partially intercalated sample was removed from the electrolyte, washed well in acetone to remove all electrolyte and then taken to the SEM as soon as possible. Scanning of the sample was started generally within 30 to 40 minutes after the intercalation stopped.

3.3 Room temperature X-ray fluorescence study of stage 1 and stage 2 TiS_2 intercalated with silver

The relative intercalated silver content as a function of distance in from the crystal edge was determined by XRF scans along a line perpendicular to the edge of the crystal. It was determined by XRF that the concentration of silver along a line parallel to the crystal edge was essentially constant. The scans were point measurements taken about 5 to 20 μm apart and the spot size sampled was typically about 2 μm across. The counting time per point was typically about 3 minutes. An XRF scan took typically about 2.5 to 3 hrs. It is very important to choose a crystal region for XRF scanning that is free of pin holes, cracks or steps because such defects allow intercalation from regions other than the crystal edge of interest. Using sample photographs and the corners of the crystals as reference points, it was possible to scan from the same place on the crystal edge repeatedly, with an accuracy of 1 to 2 μm.

The relative content of silver plotted against the distance from the edge for a typical partially intercalated crystal (sample #1) 0.9 μm thick is shown in Fig.3.4. To study the motion of the silver after partial intercalation, repeated XRF scans were carried out and Fig.3.5 shows a series of scans taken on sample #1 at room temperatures. It is seen that the stage 1 region is reduced in size and the stage 2 region is increased in size. After a sufficient time, only stage 2 silver was found in the crystal.

In sample #1 no subsequent motion of stage 2 silver was observed over a period of 2 months. This was also observed in several other samples for periods up to 2 1/2 months.

Some samples with both stages were left in liquid nitrogen for about a day and the position of the fronts were observed optically before and after leaving the sample in the liquid nitrogen. It was found that silver in both stages remained stationary.

3.4 Study of the motion of the stage 2 silver front in TiS_2 at elevated temperatures

Since no motion of the stage 2 front was observed at room temperature (that is the silver distribution in stage 2 remained constant), some samples were heated in an argon atmosphere and the distribution of silver was determined after each heating by XRF at room temperature. A sample (#2, thickness = 1.2 μm) was initially kept at 100 °C for one day. It was observed that the silver distribution or the stage 2 front had moved a few microns (10 μm) into the empty crystal but there was no change after further heating for 3 days at 100 °C. It was also found that when the sample was left at room temperature for about a week after this heating, the stage 2 front moved back to the position prior to heating. Another sample (# 3 , thickness = 2 μm) was heated at 150 °C for 1 day and it was observed that the stage 2 front had moved about 10 μm. The same sample was heated at 150 °C for another 8 days and the distribution of silver was determined each day. In this period the stage 2 front moved about 12 μm but the shape of the front was essentially unchanged. Since no motion was observed even after heating the sample # 3 continuously at 150 °C for another 10 days, the temperature was increased in intervals of 10 degrees up to 200 °C ; the sample being held at each temperature for 1 day. As the

temperature was increased the concentration decreased slightly in the whole stage 2 region and after the heating at 200 °C no stage 2 front was observed and the silver was distributed throughout the crystal. Another sample (#4, thickness = 1.2 μm) was heated at various temperatures from 100 °C to 325 °C, keeping the heating time at each temperature at two hours. The temperature was increased in 10 °C intervals and after every heating the sample was scanned to determine the silver distribution. Some of these distribution curves are shown in Fig.3.6. Graph (b) shows the distribution of stage 2 silver at room temperature. As the temperature increased the stage 2 front moved into the crystal and the steepness of the front decreased. In this sample the silver was distributed throughout the crystal after heating at 325 °C for two hours.

As shown in Fig.3.6 (f), (g) and (h) the silver concentration in a region about 15 μm from the crystal edge is lower than the other region of the same graph. The edge was scanned to find out whether any silver had come out of the crystal while heating. No silver was found on the edge of the crystal.

3.5 Discussion of the results

The XRF technique clearly demonstrates the staging of silver intercalated in TiS_2 and the motion of the stage 1 and stage 2 fronts. The series of graphs in Fig.3.5 shows the room temperature disappearance of stage 1 silver with time. It is clear from the areas under the stage 1 and stage 2 curves the stage 1 silver becomes stage 2 silver. The areas under the initial and final graphs differ only by 1% from each other. Though the depletion of the stage 1 region occurred within hours at room temperature, the stage 1 front remained stationary at liquid nitrogen temperature. When stage 1 was not present in the crystal the motion of the stage 2 front was

found only at temperatures higher than room temperature. From all these results it is clear that movement of silver atoms in the TiS_2 lattice is very temperature dependent.

Since the conversion from stage 1 to stage 2 occurs very rapidly at room temperature, this process must be driven by strong repulsive forces, presumably Coulomb forces between charged silver ions. In stage 1 ($x = 0.4$), the Ag-Ag distance is about 5.9 Å in the layers and about 6.4 Å across the layers, so that significant Coulomb repulsion can be expected from both intralayer and interlayer interactions for stage 1. For stage 2 the ion separation within a layer is the same as for stage 1, however the separation of the ions in adjacent layers is about twice the separation in stage 1. Thus it appears that the main driving force in the stage 1 to 2 conversion is the Coulomb repulsion between ions in different layers.

The fact that the stage 1 front remains stationary at 77 °K indicates that some thermal activation of the silver atoms is also required for silver motion along with the repulsive driving forces. Assuming the island model, Fig.1.4 shows that the conversion from stage 1 to stage 2 involves the generation of bends in the host layers (Fig.1.4). These bends cost some elastic energy. In spite of this, the observation of stage 1 to stage 2 conversion indicates that the decrease in Coulomb energy is greater than the elastic energy expended in forming stage 2.

The graphs obtained for sample #4 in Fig.3.6 show that, as the temperature increases the entire stage 2 region from the crystal edge to the intercalation front loses some silver, indicating this is not simple diffusion. For simple diffusion one would expect to see a drop in silver content near the intercalation front as indicated in Fig.3.7 (22). The most likely reason for the decrease in silver in the whole stage 2 region is that on heating, the sample converts to a mix of stage 2 and dilute stage

1. (Dilute stage 1 in Fig.3.8 is similar to pure stage 1 except the atoms are relatively far apart.) In this case the concentration of silver in a given area can be lower than that of stage 2. The dilute stage 1 phase requires the breakup of the stage 2 islands (assuming Herold's model) and more bending in the host layers. The stage 2 to a mix of stage 2 and dilute stage 1 transformation is likely driven by intralayer Coulomb repulsion with thermal activation.

Significant motion of silver in stage 2 was observed only at elevated temperatures. The graphs in Fig.3.6 show a fairly sharp stage 2 front up to about 250 °C. The steepness of the front started to decrease above 275 °C, and near 325 °C the silver was distributed throughout the crystal. In sample # 3 the stage 2 silver was distributed throughout the crystal at a lower temperature (200 °C) possibly because the heating time for sample #3 was longer (1 day) than the heating time for sample #4 (2 hours) .

The peaks and the valleys finally obtained in the graph (h) at 325 °C, showing collection of silver in some regions, suggests a separation of phases into perhaps the stage 2 and dilute stage 1 phases.

Fig. 3.1. (a) Diagram showing a partially intercalated TiS_2 crystal.

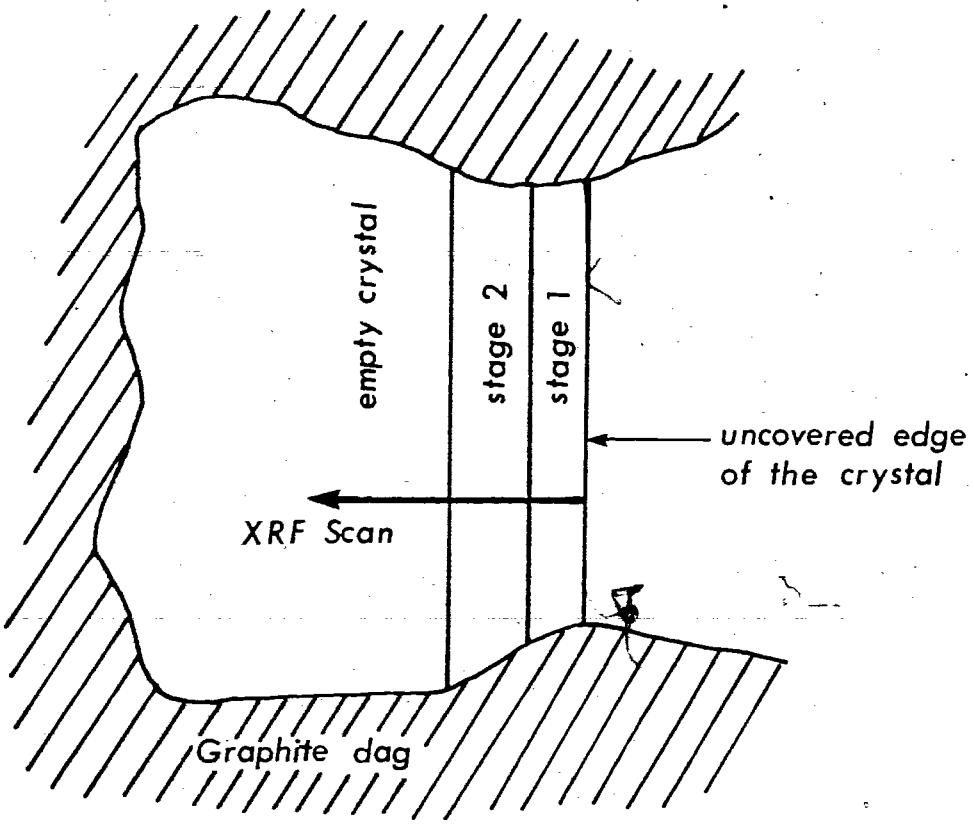
empty crystal
stage 2
stage 1
uncovered edge
of the crystal
XRF Scan
Graphite dag

Fig. 3.1 (a)

Fig. 3.1. (b) Partially intercalated TiS_2 crystal observed using reflected light.

The crystal thickness = 1.8 μm

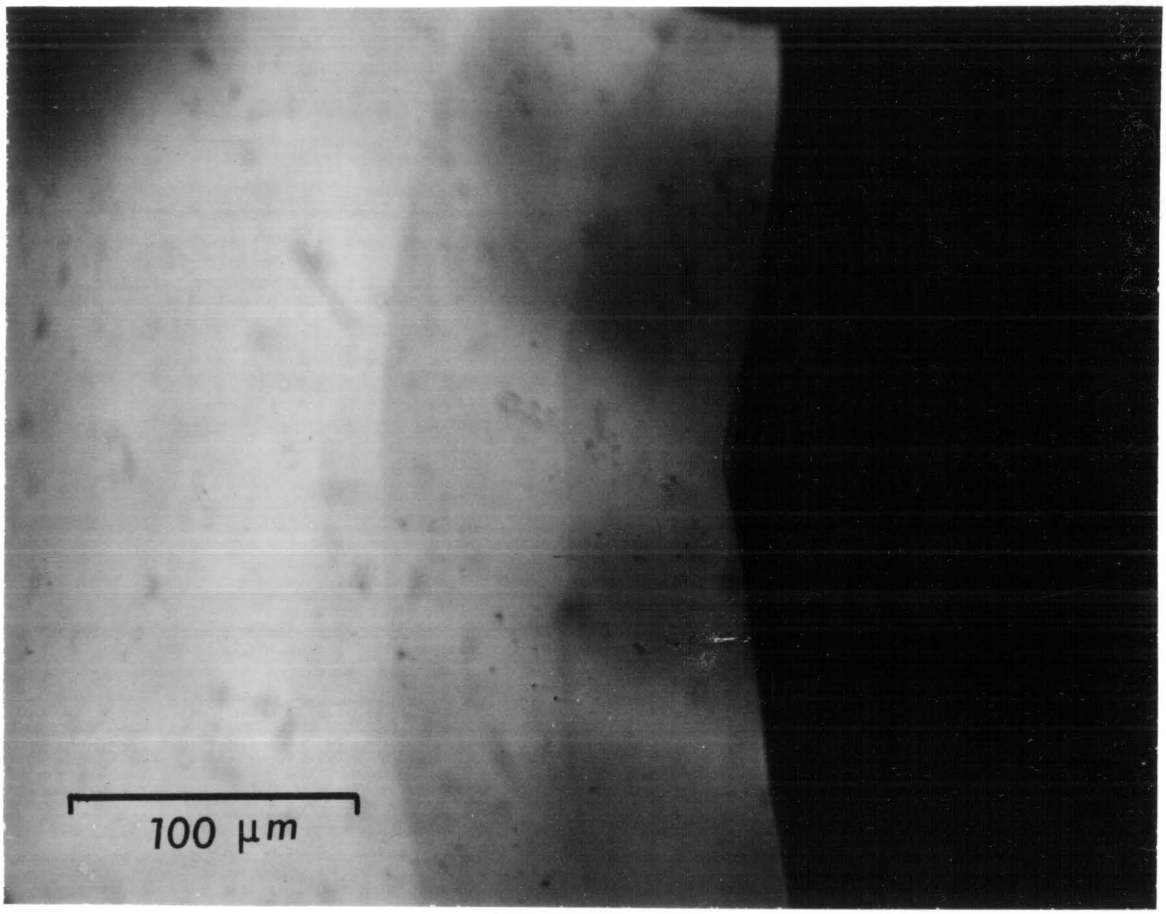

Fig. 3.1 (b)

Fig. 3.2. TiS_2 sample mounting and preparation for Ag intercalation and SEM/XRF studies.

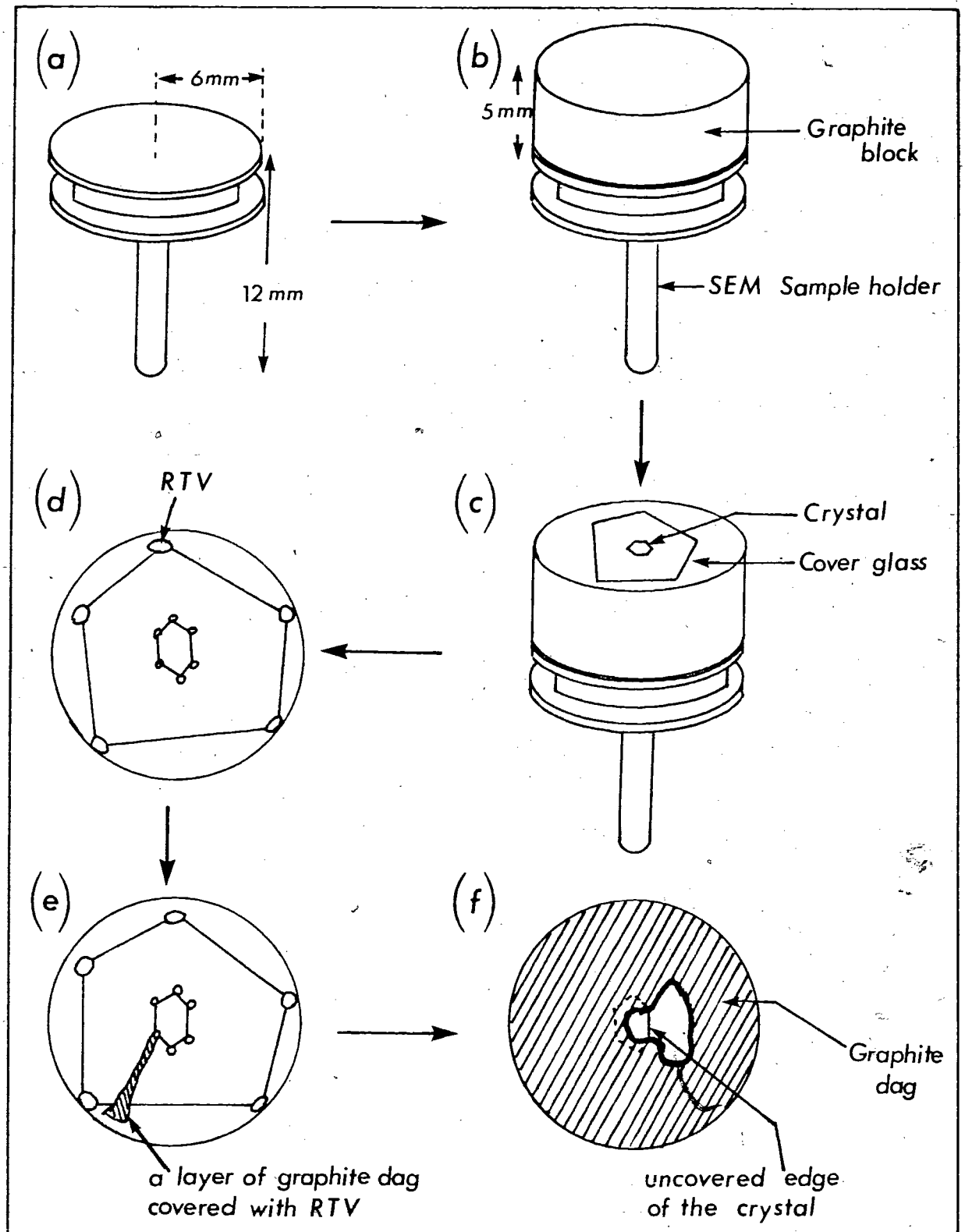
(a)
6mm
12 mm
(b)
5 mm
Graphite block
SEM Sample holder
(c)
Crystal
Cover glass
(d)
RTV
(e)
a layer of graphite dag covered with RTV
(f)
Graphite dag
uncovered edge of the crystal

Fig. 3.2

Fig. 3.3. Electrointercalation of a crystal.

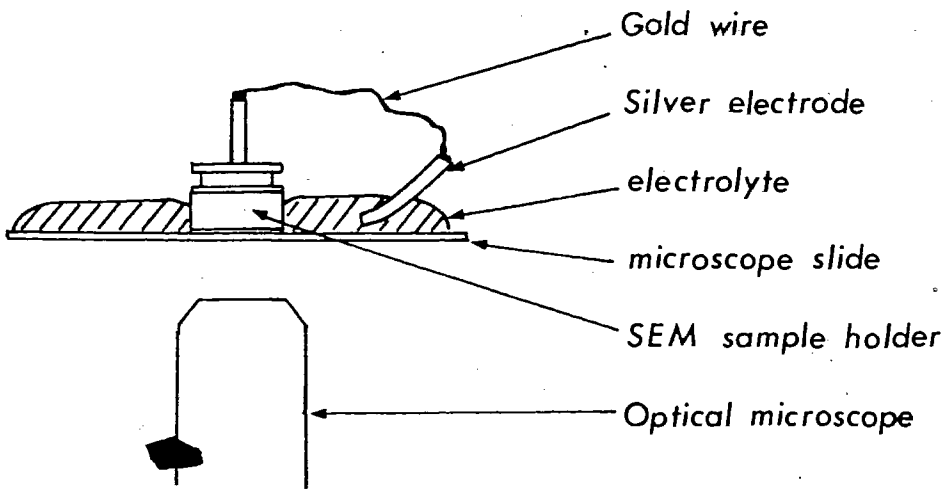
Gold wire
Silver electrode
electrolyte
microscope slide
SEM sample holder
Optical microscope

Fig. 3.3

Fig. 3.4. Distribution of Ag content in a partially intercalated TiS_2 crystal.

Crystal thickness = 0.9 μm

This scan was started 45 min. after intercalation was stopped and the total scanning time was about 2 hrs. The scan was taken from the crystal edge to the interior of the crystal.
A typical statistical error ($\sqrt{N}$) is shown for stage 1 and stage 2. In empty crystal region the error is negligible.

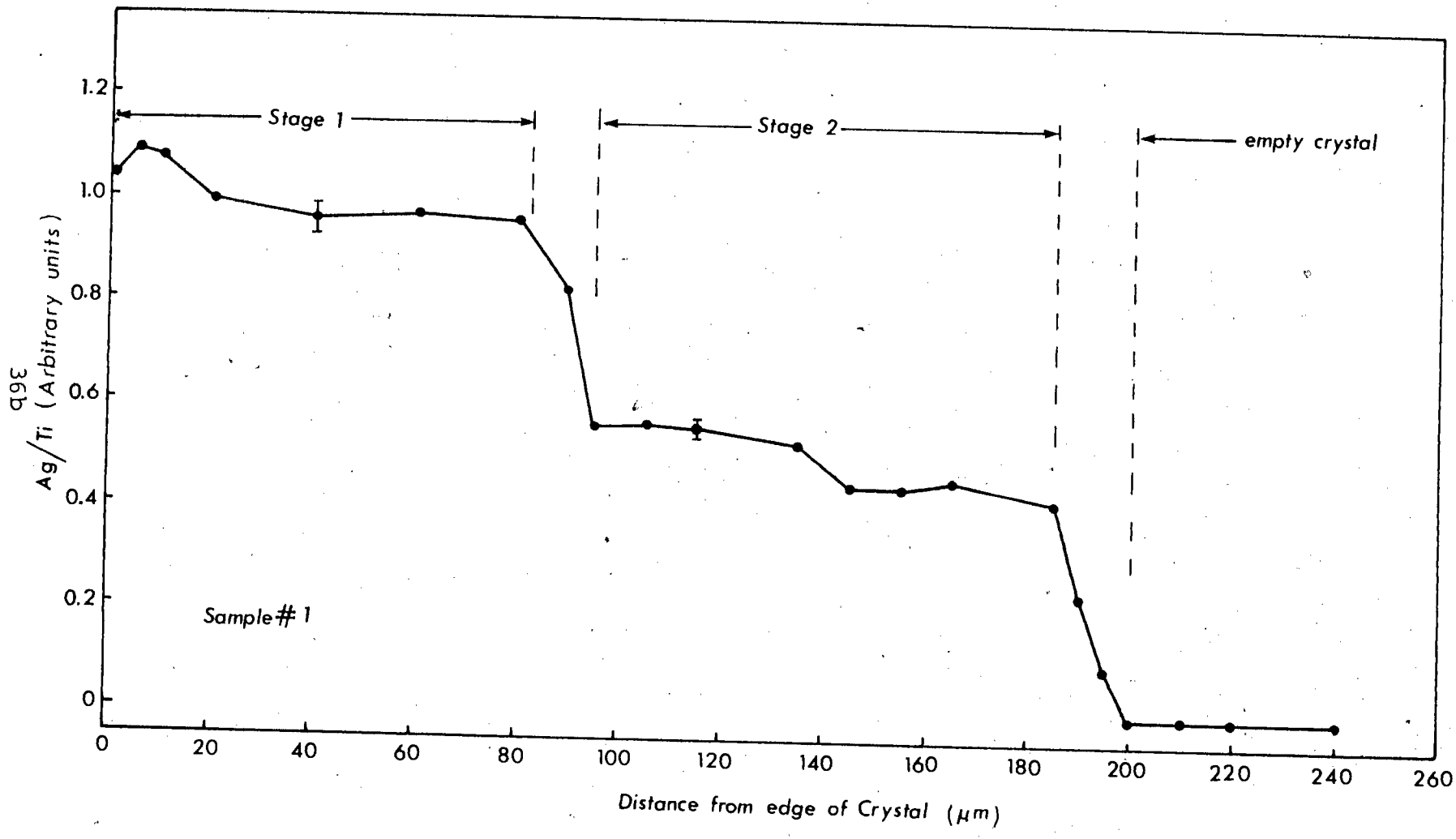
Stage 1
Stage 2
empty crystal
Sample # 1
Ag/Ti (Arbitrary units)
Distance from edge of Crystal (μm)
0
0.2
0.4
0.6
0.8
1.0
1.2
0
20
40
60
80
100
120
140
160
180
200
220
240
260

Fig. 3.4

Fig. 3.5. Distribution of Ag content in a partially intercalated TiS_2 crystal at room temperature.

The scans were taken from the crystal edge to the interior of the crystal. The series of graphs show a reduction of stage 1 and an increase in the extent of stage 2.

Time after intercalation:

(a) ○ - 45 min.

(b) ● - 2 3/4 hrs.

(c) △ - 4 1/4 hrs.

(d) + - 6 1/2 hrs.

(e) □ - All stage 1 silver has moved. (Data taken after two days.)

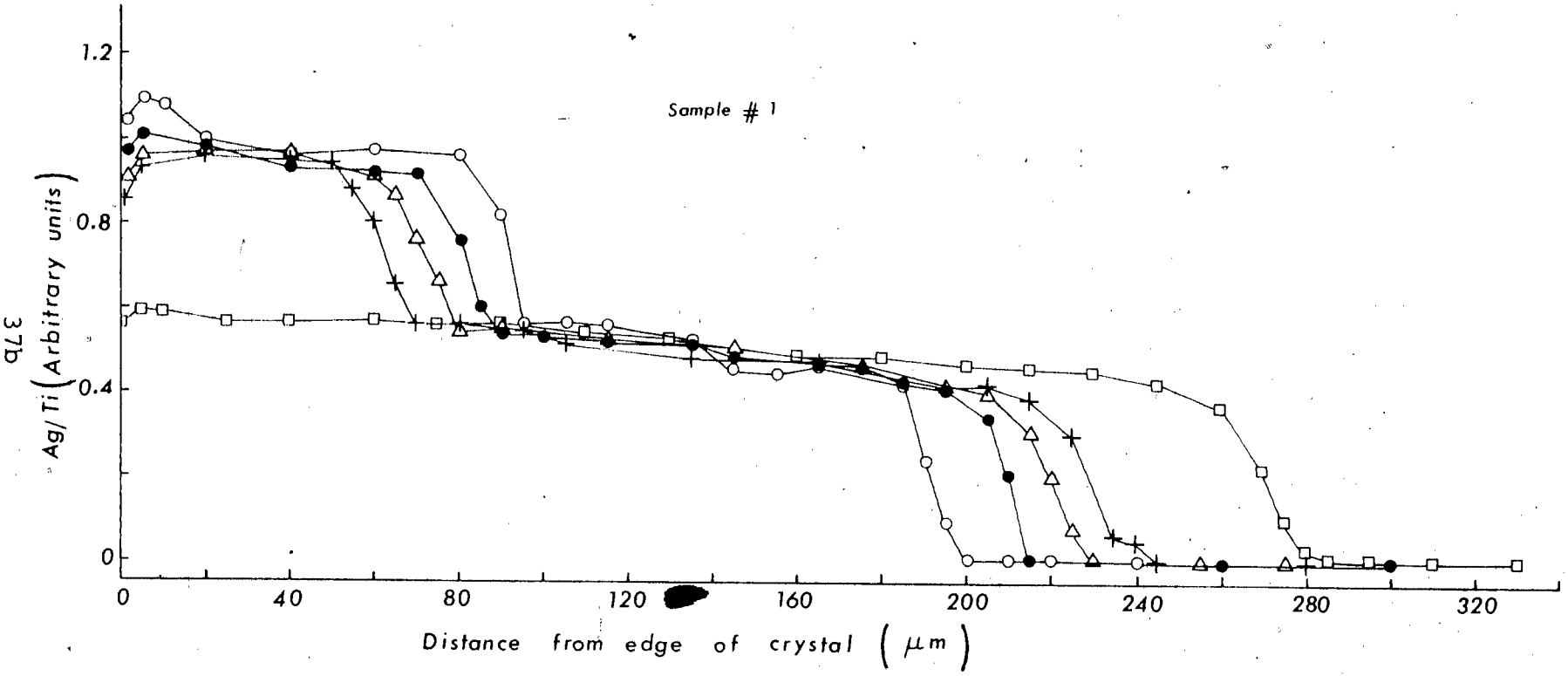
Sample # 1
Ag/Ti (Arbitrary units)
1.2
0.8
0.4
0
0
40
80
120
160
200
240
280
320
Distance from edge of crystal (μm)

Fig. 3.5

Fig. 3.6. Temperature dependence of motion of stage 2 silver in TiS_2.

Crystal thickness = 1.2 μm

Time after intercalation:

(a) ○ - 1 hour : room temperature

(b) ▷ - After all stage 1 silver has moved into stage 2 silver : room temperature

After heating for 2 hours:

(c) ✳ - 100 °C

(d) ◇ - 150 °C

(e) ▲ - 200 °C

(f) ⊙ - 275 °C

(g) □ - 300 °C

(h) ● - 325 °C

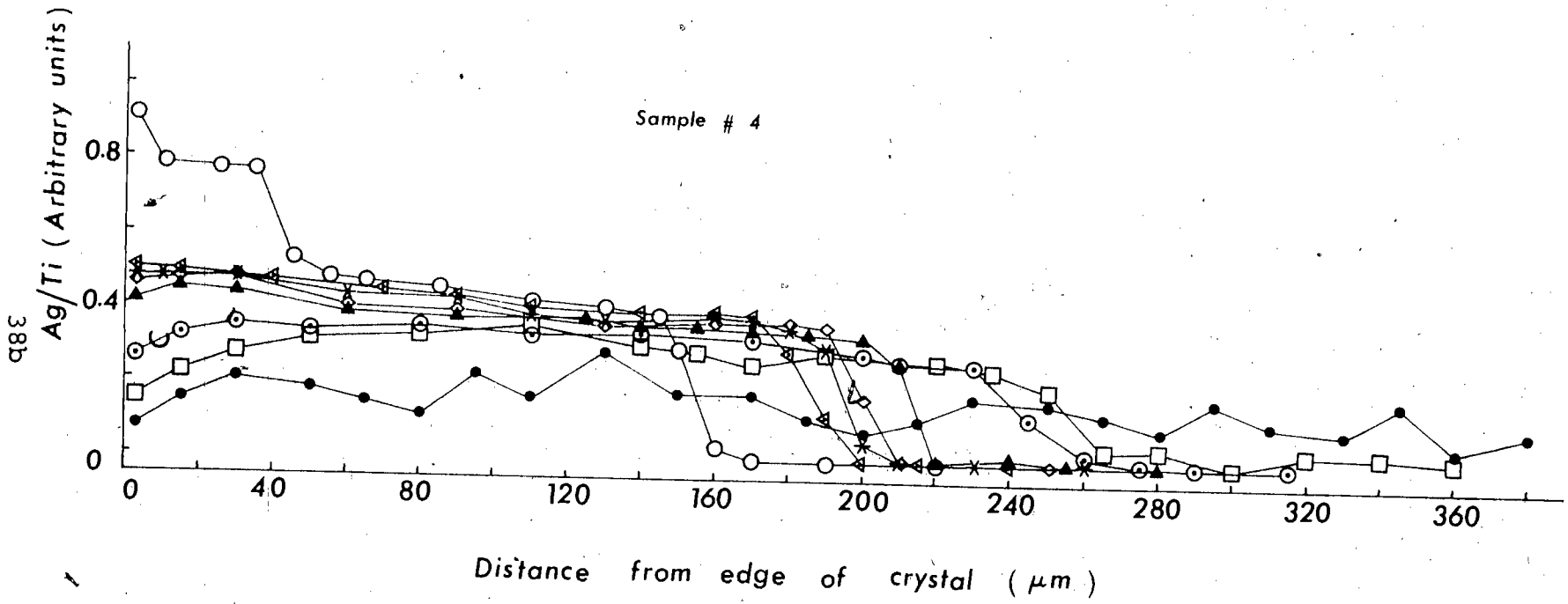
Sample # 4
Ag/Ti (Arbitrary units)
0.8
0.4
0
0
40
80
120
160
200
240
280
320
360
Distance from edge of crystal (μm)

Fig. 3.6

Fig. 3.7. General form for diffusion curves starting with a sharp boundary (15).

Fig. 3.8. Dilute stage 1

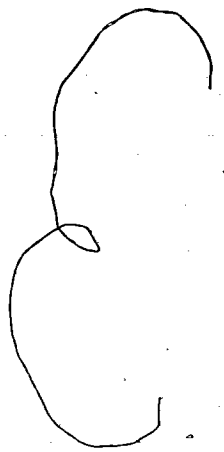

——— host layer

• • • guest layer

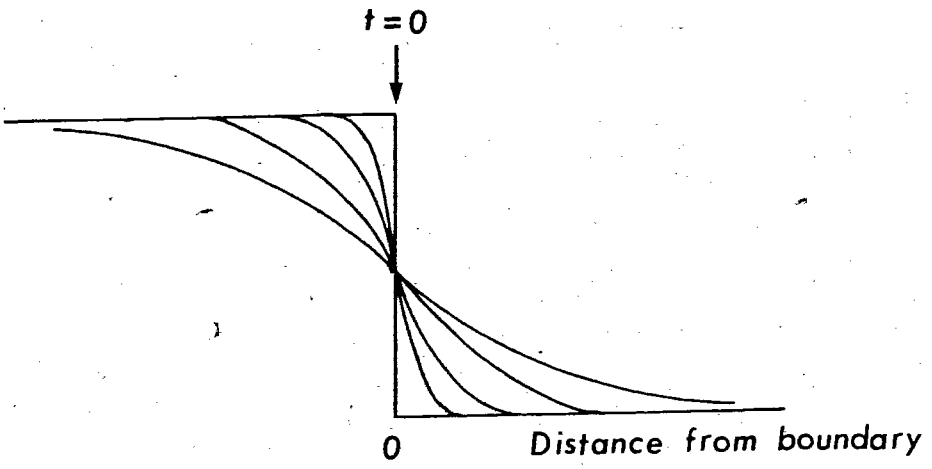

Fig. 3.7

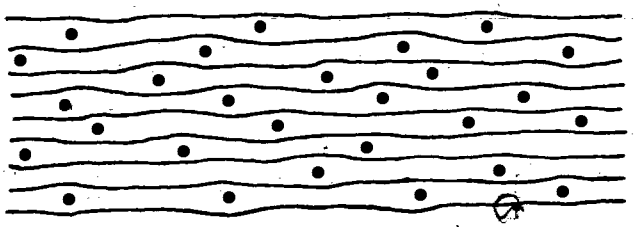

Fig. 3.8

IV. Intercalation of TiS_2 with Ag^{108} and Ag^{110}.

Some experiments were done with radioactive silver (Ag^{110}) to clarify how the motion of silver occurs in TiS_2 for both stage 1 and stage 2 at room temperature.

4.1 Study of migration of Ag in stage 2 when a crystal is intercalated

A radioactive tracer experiment was done to study the migration of silver atoms in stage 2 when a crystal is intercalated. When a crystal intercalates a stage 2 front is observed (optically) to start first, followed by a stage 1 front. If the concentration of the electrolyte is decreased a stage 1 front is not observed. Thus it is possible to obtain only a stage 2 region in a crystal, except perhaps right at the crystal edge, by limiting the intercalation rate using a low electrolyte concentration. In the experiment in this section, the crystals were partially intercalated such that only stage 2 was obtained.

The question to be answered by the tracer experiment was: Where do the silver atoms go after they enter a partially intercalated stage 2 crystal? Three possibilities are shown in Fig.4.1 for the classical intercalation model.

For Fig.4.1:

(a) The newly intercalated silver atoms push the preintercalated silver atoms further into the crystal and remain near the edge of the crystal.

(b) The newly intercalated silver atoms advance to the stage 2 front by moving past stationary preintercalated silver atoms (the new atoms are not necessarily in the same layers as the preintercalated atoms).

(c) As in (a) with the preintercalated atoms and the new atoms mixed together near the interface.

In our experiments, radioactive Ag^{110} was used to label the new silver atoms. A crystal was first intercalated with nonactive Ag^{108} and then was intercalated with active Ag^{110}. Intercalation was done so that only stage 2 was formed, leaving the inner part of the crystal empty. After intercalation the total activity of the crystal was measured. Then the edges of the crystal were cut and the activities of all edges and the inner part of the crystal were measured separately.

Ag^{110} emits a wide spectrum of gamma radiation, 95% of which is 657 keV gamma rays (23). To measure the crystal activity, the whole gamma spectrum ($E \geq 100$ keV) was detected with a NaI well-type scintillation spectrometer (Fig.4.2) in the Department of Chemistry, S.F.U.

4.1.1. Sample preparation and intercalation: motion of stage 2 silver

Since the amount of silver intercalated and hence the activity increases with thickness it is advantageous to use the thickest crystals available in counting experiments. However thick crystals tend to crack while they are being intercalated. It was found by trial and error crystals in the thickness range 3 to 6 μm did not crack severely and gave reasonable counting statistics.

As described in section 3.2 crystals were peeled from grown TiS_2 crystals and placed on cover glasses where the thicknesses were measured. In our experiments it was very important to use crystals without cracks, pin holes, steps, scratches or any other macroscopic defect. It was possible to observe intercalation due to such defects on the upper surface, however the lower surface could not be observed after mounting the crystal. Therefore before mounting the crystal a thin layer of RTV (silicone rubber) was spread on the lower surface (but not near the crystal edges) to prevent any possible intercalation at defects. Prior to intercalation any

small defects on the upper surface were carefully covered with tiny dots of RTV. The next steps in sample preparation are shown in Fig.4.3. A piece of cover glass with a crystal was placed on a sample holder as shown in Fig.4.3 (a). (A SEM sample holder was used only for convenience.) The corners of the crystal were held to the glass by RTV (Fig.4.3 (b)),and a very small piece of silver was fixed to the crystal with some silver dag (Electrodag 415 from Acheson Colloids). This silver dag was then covered with RTV to ensure a contact with the crystal was maintained. Finally an electrolyte container was made using a small rubber 'O' ring (Fig.4.3 (c)). Since a radioactive electrolyte was used a minimum amount of the electrolyte was desirable. The idea of using a small 'O' ring was to make a very small well to hold the electrolyte. The top cover glass was placed on the 'O' ring to prevent evaporation of the electrolyte. The sample preparation was done under an optical microscope. Basically, the set up shown in Fig.4.3 (d) is similar to Fig.3.3. The intercalation process was observed in reflected light with an optical microscope, keeping the sample holder upright.

The electrolyte was prepared from a solution of 0.1 M Ag^{110} in 0.5 M HNO_3 in water, purchased from New England Nuclear of Canada. The radionuclidic purity and the radiochemical purity of the original solution was about 99%. In our experiment a solution of 0.001 M Ag^{110} in 0.05 M HNO_3 in water was used as the active electrolyte. The nonactive electrolyte was made up with the identical molarity and solvent as the active one. The volume of the electrolyte in a cell was about 55 microliters and the activity of this amount of electrolyte was about 0.01 μCi.

It was mentioned in section 3.2.2 that a considerable amount of cracking was observed at the crystal edge when an aqueous electrolyte was used for intercalation. However, in the tracer experiment where aqueous

electrolytes were used few cracks were observed in the crystal edge since the intercalation rate was slow due to the low concentration of the electrolytes. In the radioactive tracer experiment the crystals were intercalated at all of the edges as follows. A crystal was first intercalated with nonactive silver until the stage 2 front moved a distance x, typically about 60 to 100 μm from the crystal edges (Fig.4.4 (a)). Then the crystal was photographed and washed with acetone to remove the electrolyte. Next the crystal was again intercalated with the active electrolyte until the stage 2 front progressed a further distance z, typically about 30 to 40 μm into the crystal giving a total stage 2 width of y (Fig.4.4 (b)). With photographs it was possible to measure the widths x and y of the stage 2 region as indicated in Fig.4.4. Since the boundary of the active and nonactive regions could not be observed optically, z was calculated from the values x and y. The crystals were always intercalated such that $x > (y - x) = z$. Then $y > 2z$ and therefore it was possible to cut the edges of the crystal such that the widths of both the cut sections and of the remaining stage 2 region in the middle part was greater than z (Fig.4.5 (b)). The reason for doing this will be explained later in Fig.4.6. After intercalating the crystal with active silver, the electrolyte was washed away and the crystal was removed from the sample holder. This was done under a microscope with fine tools. Then the crystal was again washed thoroughly with acetone to get rid of any remaining electrolyte on the surfaces and taken to the counter to measure the crystal activity. The background radiation was counted for one hour and the counting for the crystals was 20 minutes. The procedure used to monitor the location of active silver in a crystal was as follows. The total crystal activity was first measured and then the narrow sections of the crystal edges were cut with a razor blade as shown in Fig.4.5 (b). Using a

microscope, it was possible to make cuts with an accuracy of about +/- 10 μm. After cutting, all the cut sections were collected carefully with fine forceps and the total activity of all the sections was determined. The activity of the remaining middle part of the crystal was also measured.

Three possible distributions for the new guest atoms corresponding to the silver location of Fig.4.1 are shown in Fig.4.6. In our experiment the new guest atoms are active Ag^{110} atoms and the preintercalated atoms are nonactive Ag^{108} atoms. From the measured activities one can obtain information on the distribution of Ag^{110} in the crystal. If Fig.4.6 (a) is the case, the active silver will reside near the crystal edge and the activity of the whole crystal should be the same as the total activity of the cut sections. If what is shown in Fig.4.6 (b) happens, the activity of the middle part of the crystal should be the same as the total crystal activity. For the case in Fig.4.6 (c) most of the total crystal activity should be found in the cut sections and the middle part of the crystal will also show some low activity.

4.1.2 Results of migration of stage 2 silver

Results for two samples studied are shown in Table 4.1. The values given in the table are the counts after the background of 9.30 +/- 0.05 cps was subtracted. Note that the sum of counts from the cut sections and the middle region is close to the counts from the original crystal indicating that no sections were lost during the cutting procedure. It is clear from the results that most of the active silver atoms reside in the cut sections of the crystal. A low but not negligible activity was found in the middle part, so there is no sharp boundary between the active and nonactive regions.

4.2 Study of conversion of stage 1 silver into stage 2

As presented in chapter 3 it was observed that when intercalation of a partially intercalated crystal is stopped the stage 1 silver region rapidly disappears with the intercalated region converting into stage 2. It is of interest to know how this stage 1 to stage 2 conversion occurs. That is, how do the silver atoms redistribute during the stage conversion? The most likely situations are given Fig.4.7. In stage 1, all the layers of the host lattice are filled with silver while in stage 2 region every other layer is filled. One possibility is that the excess silver in the stage 1 region advances to the stage 2 front as in Fig.4.7 (b). In this case the existing stage 2 silver is stationary while the silver from stage 1 moves through it. In Fig.4.7 (c) the silver in stage 1 pushes the existing stage 2 silver into the empty region of the crystal and remains near the crystal edge. Fig.4.7 (d) is similar to Fig.4.7 (c) except the silver from both stages are mixed together near the stage 1 - stage 2 boundary.

In the follwing sections, a radioactive tracer experiment is described which allows the silver motion to be follwed. In this experiment Ag was used to label the silver in the stage 1 region.

4.2.1 Sample preparation and intercalation: motion of stage 1 silver

The preparation of partially intercalated samples was essentially the same as described in section 4.1.1. The nonactive elctrolyte used was a solution of 0.01 M $AgNO_3$ in 0.05 M HNO_3 acid. The active electrolyte was a mixture of Ag^{110} and Ag^{108} with a molarity 0.01 M in 0.05 M HNO_3 acid. Some nonactive Ag^{108} solution was mixed with the active solution to reduce the high activity.

In this experiment it was necessary to intercalate the sample in both stages such that $q > 2p$ (Fig.4.7 (a)). A wide band of stage 2 Ag^{108} was needed so that a crystal was first intercalated with nonactive silver until both stage 1 and stage 2 were obtained; intercalation was stopped and the cystal was left until the stage 1 silver was converted into stage 2, giving a final total stage 2 width typically about 100 to 130 μm. After obtaining a wide region of stage 2 Ag^{108} the crystal was photographed and again intercalated with Ag^{108} until the stage 1 front was just observed at the edge. Then the electrolyte was quickly changed to the active Ag^{110} solution. This procedure ensured that Ag^{110} atoms were intercalated only in the stage 1 region. Intercalation with Ag^{110} was continued until the stage 1 front was observed to be a distance p wide (typically 30 to 50 μm). After intercalation the crystal was again photographed and the electrolyte was washed away. The crystal then was removed from the sample holder, washed again and left for about a day to allow the stage 1 Ag^{110} to convert into stage 2 Ag^{110} .

After the stage 1 was converted to stage 2 the total crystal activity was counted and crystal sections were cut with a razor blade at a distance a little more than 2p from the crystal edges. The activity in the cut sections and the remaining part of the crystal was measured separately. The results showed that most of the active atoms were located in a region 2p from the crystal edges. As was observed in the experiment described in section 4.1 some activity was measured in the remaining crystal so that strips (typically 30 to 40 μm) were again cut from the crystal and the activity in these strips and remaining crystal were measured.

To confirm the results of this experiment another experiment was done by replacing the nonactive electrolyte with the active electrolyte and vice versa.

4.2.2 Results of migration of stage 1 silver into stage 2

The results of migration of stage 1 silver for two samples are given in Table 4.2 and Table 4.3. The values given in the tables are counts after the background is subtracted. It can be seen that after the motion of stage 1 silver most of the active silver atoms were found near the edge of the crystal and no significant activity was measured in the remaining part after the second cut.

When the electrolytes were interchanged, that is when stage 2 was obtained with Ag^{110} and the stage 1 with Ag^{108} the converse result was found (Table 4.4). That is, most of the active Ag^{110} was found near the final stage 2 front and there was no significant activity in the sections cut off by the first cut. A slight activity was found in cut off sections of the second cut showing the consistency of the results given in Tables 4.2, 4.3 and 4.4.

4.3 Discussion of the results

The tracer results from section 4.1.2 where the migration of stage 2 silver was studied show that when silver atoms enter a partially intercalated stage 2 TiS_2 crystal the preintercalated atoms are effectively pushed further into the crystal by the entering silver atoms. That is, all the silver in stage 2 moves when the crystal intercalates. The XRF results in chapter 3 show that, after intercalation ceases, silver in stage 2 remains stationary when stage 1 is not present in the crystal. So that when a crystal intercalates, the overall driving energy for stage 2 may be derived from a very narrow region of stage 1 at the edge of the crystal.

The tracer results in section 4.2.2 where the motion of stage 1 silver was studied show that when intercalation of a partially intercalated

crystal is stopped, the silver in stage 1 pushes stage 2 silver into the crystal and stays near the edge giving a distribution of silver similar to Fig.4.7 (d).

Fig.4.8 shows the distribution of Ag^{110} in the samples #3 and #4 after stage 1 Ag^{110} has moved. These graphs were plotted by equating the ratio of measured activities in cut sections to the ratio of the areas under the curves in the corresponding regions. Since the width of the initial stage 1 Ag^{110} front was p, we assumed that only Ag^{110} is found within a distance p from the crystal edge and Ag^{110} may or may not mix with Ag^{108} beyond p. Since the Ag^{110} in the distribution was initially in the stage 1 region of width p the conservation of Ag^{110} in the crystal was taken into account. To satisfy all these conditions, the widths of the initial stage 1 fronts (p) and the cut sections of the crystals were changed within the experimental errors in some cases. In sample #3 the width of the stage 1 region used was 45 μm and the width used for the first cut was 95 μm. In sample #4 the width used for the first cut was 95 μm and the width of the second cut was 40 μm. Additionally, the activities were changed slightly within the experimental errors.

Some activity was found beyond the expected region (2p) which is consistent with Fig.4.7 (d). This observation also agrees with XRF results where it was observed that intercalation fronts are not absolutely sharp and that the stage 2 front becomes wider after the conversion of stage 1 silver into stage 2 silver (Fig.3.5 and Fig. 3.6).

The results obtained in this chapter support Daumas and Herold's model of staging (chapter 1). The type of motion of stage 1 silver into stage 2 silver required by the tracer results can be explained with islands of atoms in host layers. The classical model of staging and Daumas and Herold's model of staging are shown in Fig.1.3 and Fig.1.4 respectively.

The conversion from stage 1 to stage 2 in the classical model is shown in Fig.4.9. The motion shown in Fig.4.9 is only possible if there is migration of silver atoms perpendicular to the layers. Since it was found that the motion of silver atoms perpendicular to the layers is negligible at room temperature (chapter 6), the classical model cannot explain the tracer results. The island model in Fig.4.10 explains clearly how silver atoms in stage 1 remain near the crystal edge in the stage 1 to stage 2 conversion.

Fig. 4.1. These diagrams give a set of possibilities for residing atoms in a partially intercalated stage 2 crystal.

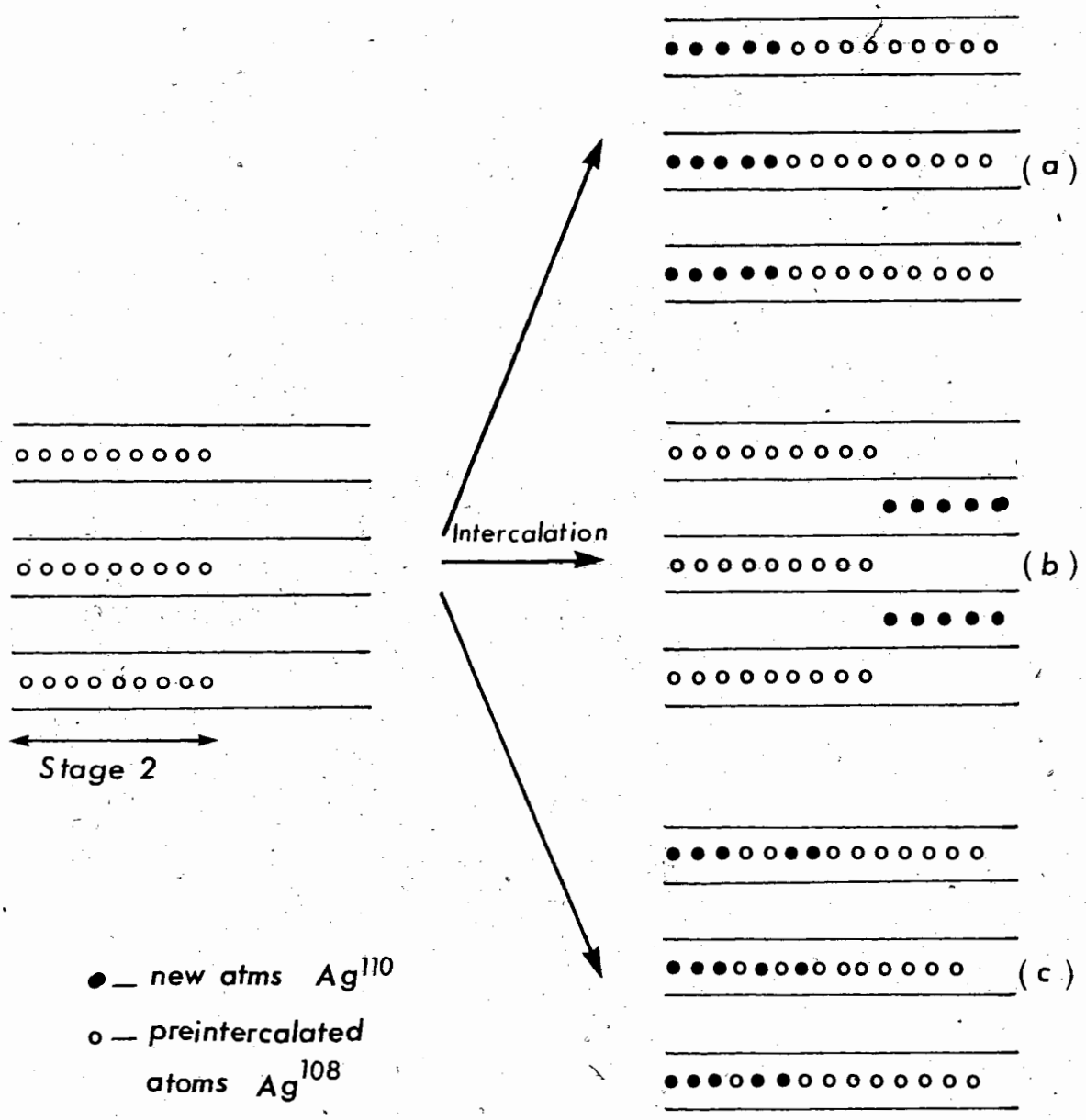
Intercalation
(a)
(b)
(c)
Stage 2
● — new atms Ag^{110}
o — preintercalated atoms Ag^{108}

Fig. 4.1

Fig. 4.2. A schematic diagram of NaI well-type scintillation detector.

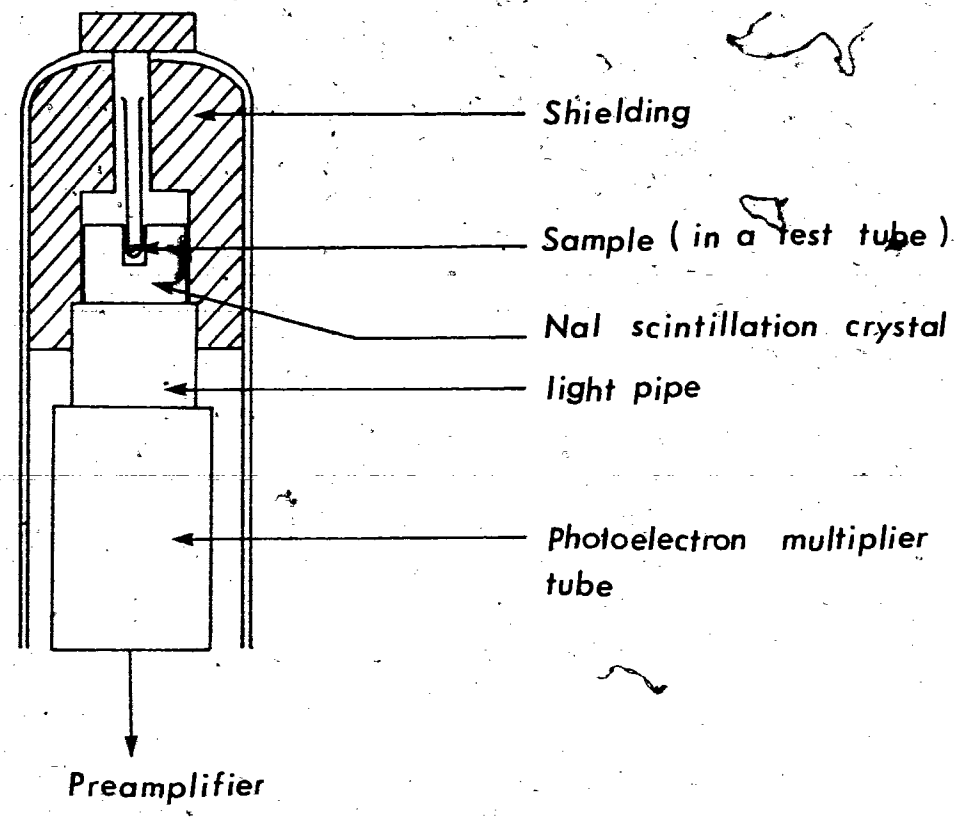
Shielding
Sample (in a test tube)
NaI scintillation crystal
light pipe
Photoelectron multiplier tube
Preamplifier

Fig. 4.2

Fig. 4.3. Sample preparation for the radioactive tracer experiment.

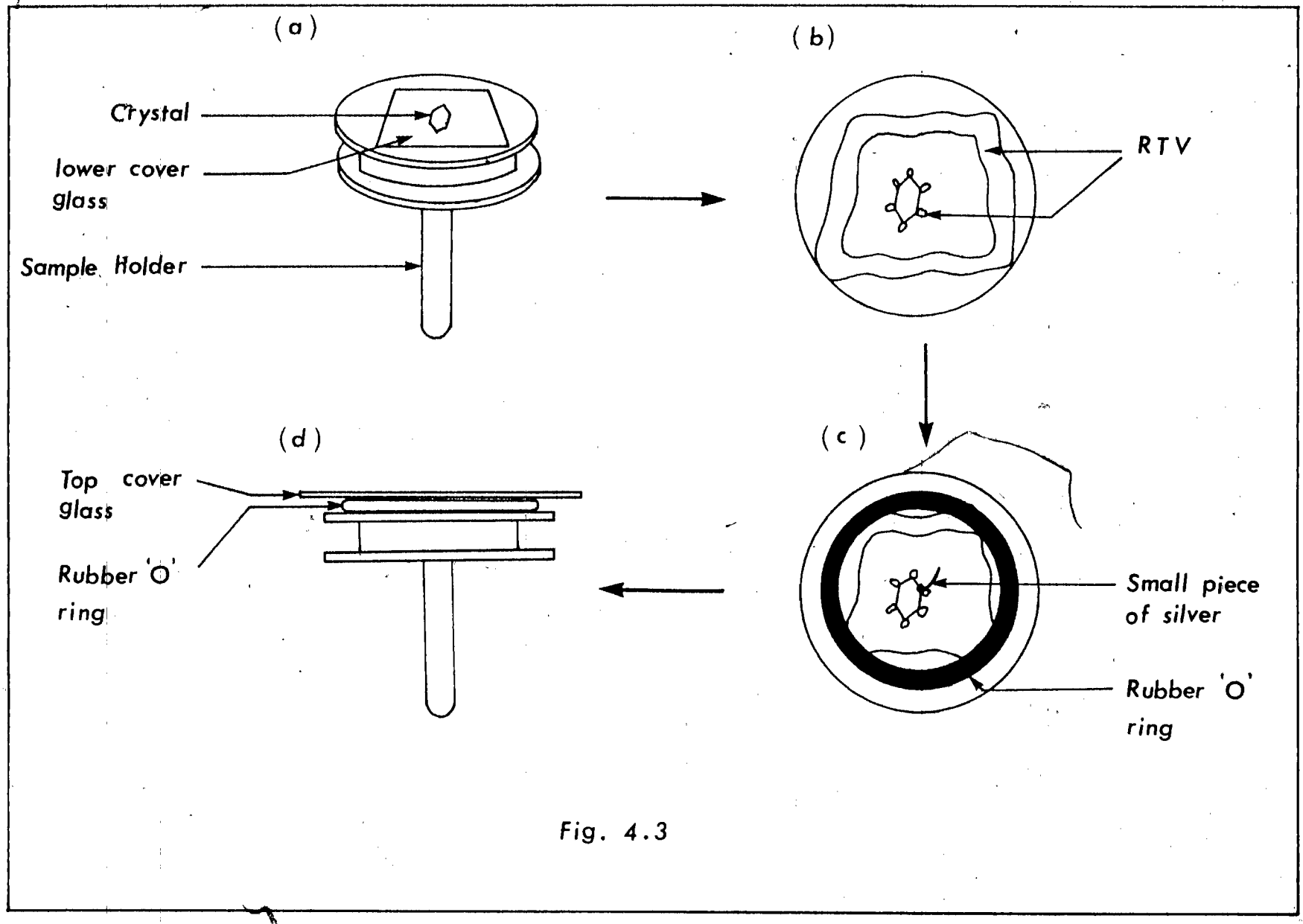
(a)
Crystal
lower cover glass
Sample Holder
(b)
RTV
(c)
Small piece of silver
Rubber 'O' ring
(d)
Top cover glass
Rubber 'O' ring

Fig. 4.3

Fig. 4.4. Stage 2 region : Intercalated with Ag^{108} and Ag^{108}.

x = Width of stage 2 region of Ag^{108}

y = Width of stage 2 region of Ag^{110} + Ag^{108}

Fig. 4.5. Cutting of the edges of the crystal.

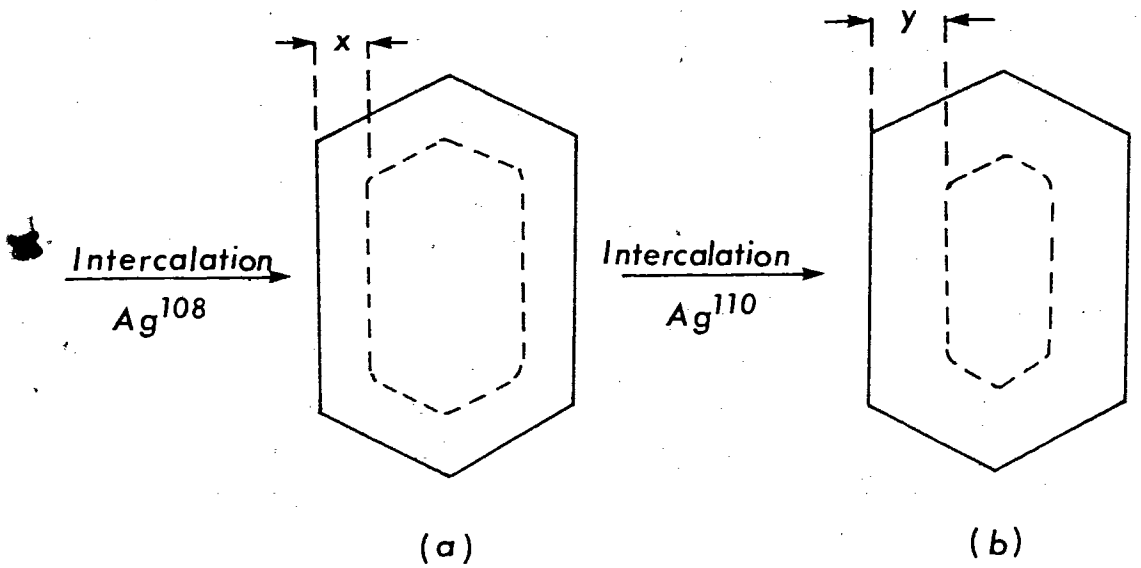
x
y
Intercalation
Ag^{108}
Intercalation
Ag^{110}
(a)
(b)

Fig. 4.4

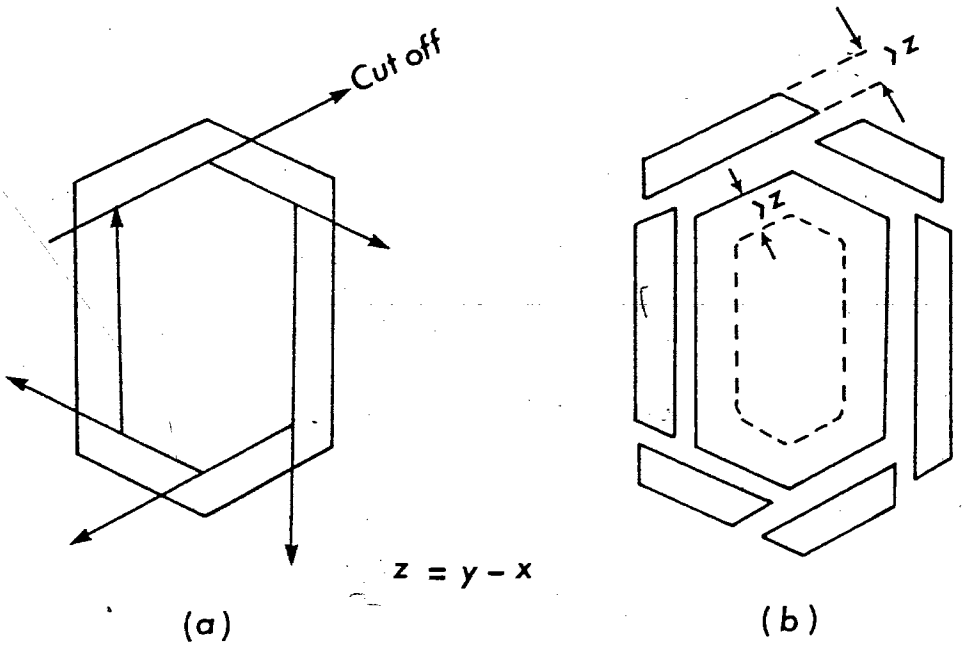
Cut off
z
z
z = y − x
(a)
(b)

Fig. 4.5

Fig. 4.6. Three possible distributions for the new guest atoms (Ag^{110}) for stage 2 intercalation.

(a) The new guest atoms (Ag^{110}) reside near the crystal edge.

(b) The new guest atoms (Ag^{110}) advance to the intercalation front.

(c) As in (a) with the guest atoms Ag^{110} and the preintercalated atoms Ag^{108} mixed at the boundary.

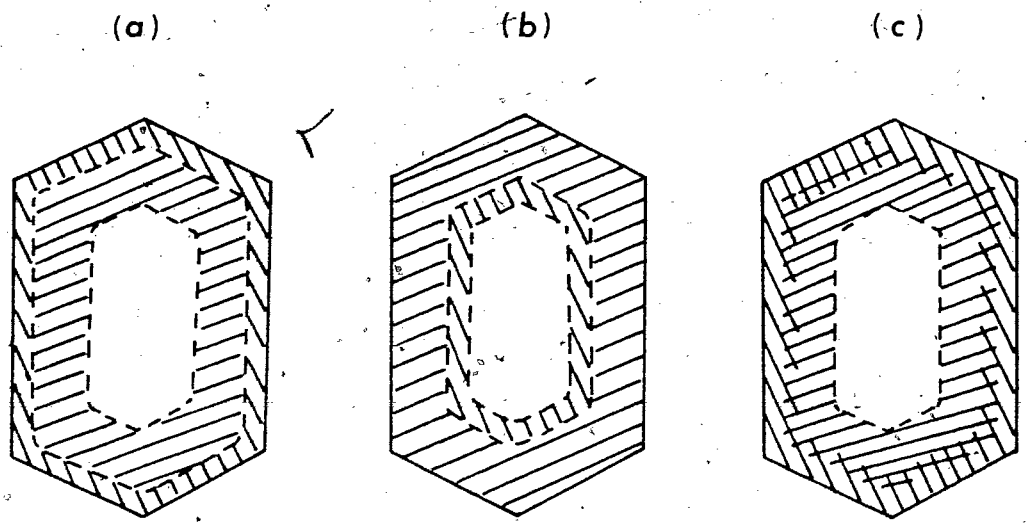

— Radioactive Ag^{110}

— Nonactive Ag^{108}

Fig. 4.6

Fig. 4.7. Possible Ag motion in the stage 1 to stage 2 conversion in a partially intercalated TiS_2.

(a) Crystal with stage 1 and 2

(b) Final stage 2 with Ag from stage 1 at crystal edge and stage 2 front

(c) Final stage 2 with Ag from stage 1 only at edge region

(d) As in (c) with Ag from both stages are mixed together near the stage 1 - stage 2 boundary

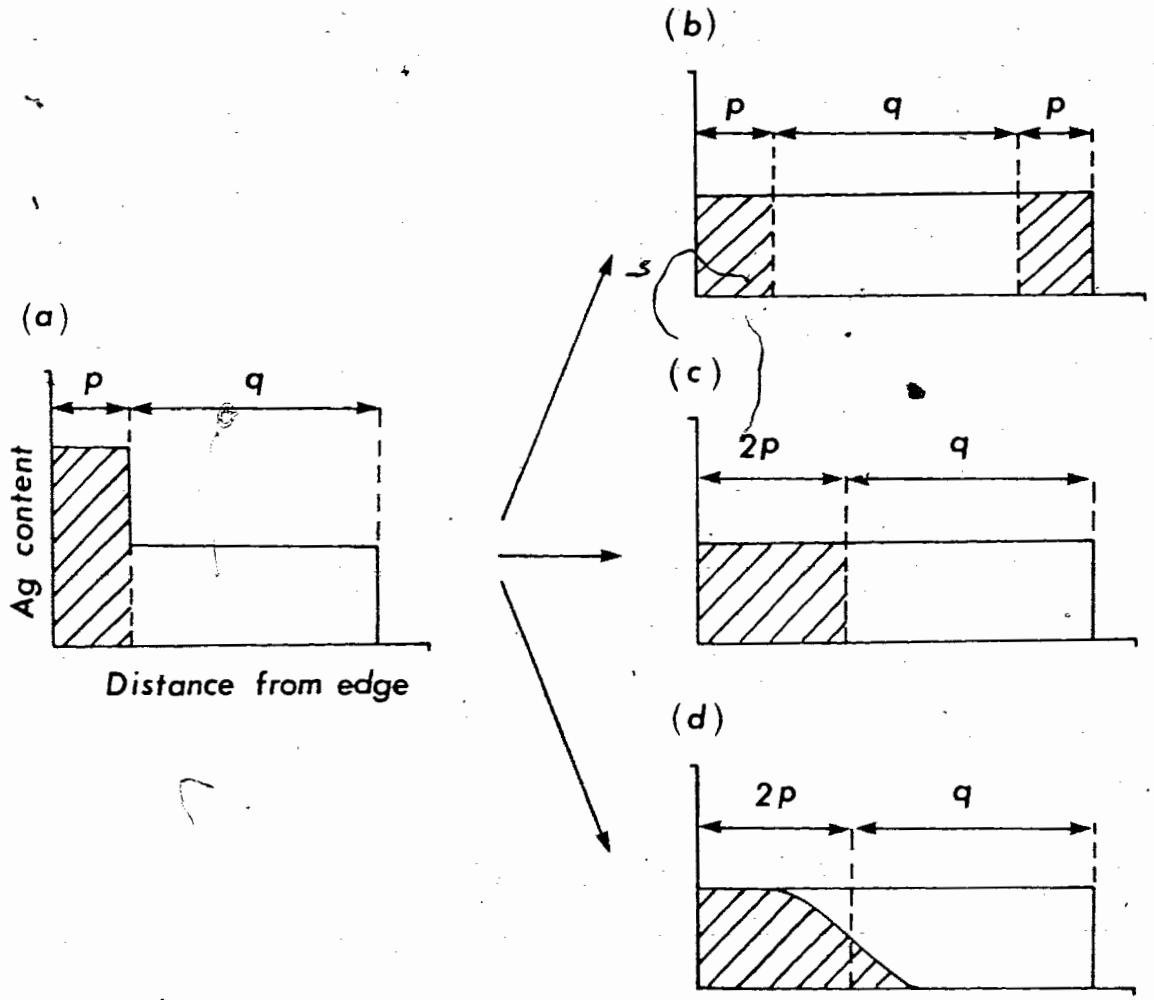
(a)
p
q
Ag content
Distance from edge
(b)
p
q
p
s
(c)
2p
q
(d)
2p
q
– Ag from stage 1
– Ag from existing stage 2

Fig. 4.7

Table 4.1. Results of Ag^{110} tracer experiment : Stage 2

Sample # 1 and # 2

Table 4.1.

Sample #	Thickness ± 0.1 μm	x ± 5 μm	y ± 5 μm	Width of cut sections ± 10 μm	Counts per second		
					Whole crystal	Cut sections	Remaining crystal
1	6.0	60	30	40	9.62 ± 0.23	8.14 ± 0.[illegible]	1.38 ± 0.18
2	5.8	80	30	40	9.13 ± 0.23	7.92 ± 0.22	1.23 ± 0.18

Table 4.2. Results of Ag^{110} tracer experiment : Conversion of stage 1 (Ag^{110}) into stage 2 (Ag^{108}).

Sample # 3

Thickness of the crystal = 5 μm

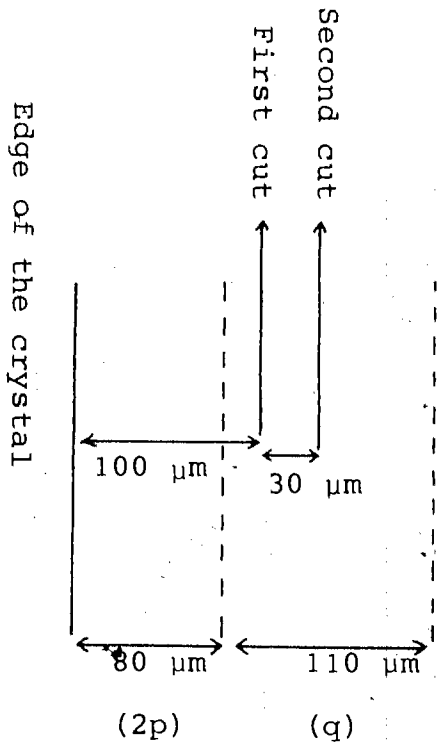

Table 4.2

p ± 5 μm Ag^{110}	q ± 5 μm Ag^{108}	2p ± 10 μm	Counts per second				
			Whole crystal	First cut Width = 100 ± 10 μm		Second cut Width = 30 ± 10 μm	
				Cut off sections	Remaining crystal	Cut off sections	Remaining crystal
40	110	80	11.88 ± 0.22	10.70 ± 0.22	1.17 ± 0.18	1.09 ± 0.18	0.20 ± 0.18

Table 4.3. Results of Ag^{110} tracer experiment : Conversion of stage 1 (Ag^{110}) into stage 2 (Ag^{108}).

Sample # 4

Thickness of the crystal = 6 μm

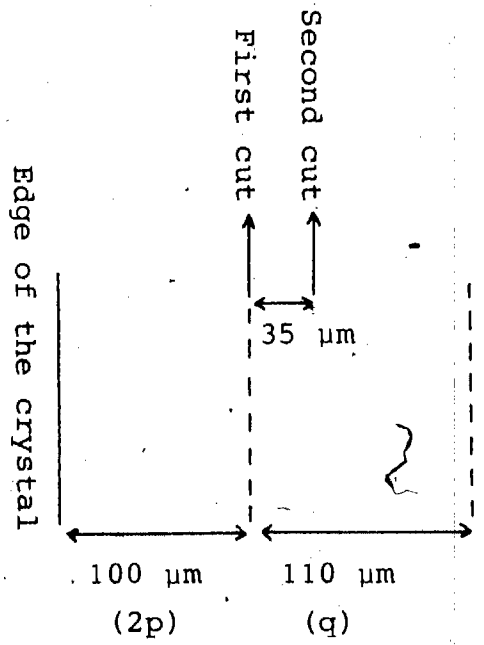

Table 4.3

p ± 5 μm Ag^{110}	q ± 5 μm Ag^{108}	2p ± 10 μm	Counts per second				
			Whole crystal	First cut width = 100 ± 10 μm		Second cut width = 35 ± 10 μm	
				Cut off sections	Remaining crystal	Cut off sections	Remaining crystal
50	110	100	15.26 ±0.23	12.72 ± 0.22	2.64 ± 0.19	2.30 ± 0.19	0.31 ± 0.18

Fig. 4.8. Construction of distribution of Ag^{110} in TiS_2 crystal.

After stage 1 Ag^{110} converted into stage 2 Ag^{110}.

Using data from Tables 4.2 and 4.3 respectively.

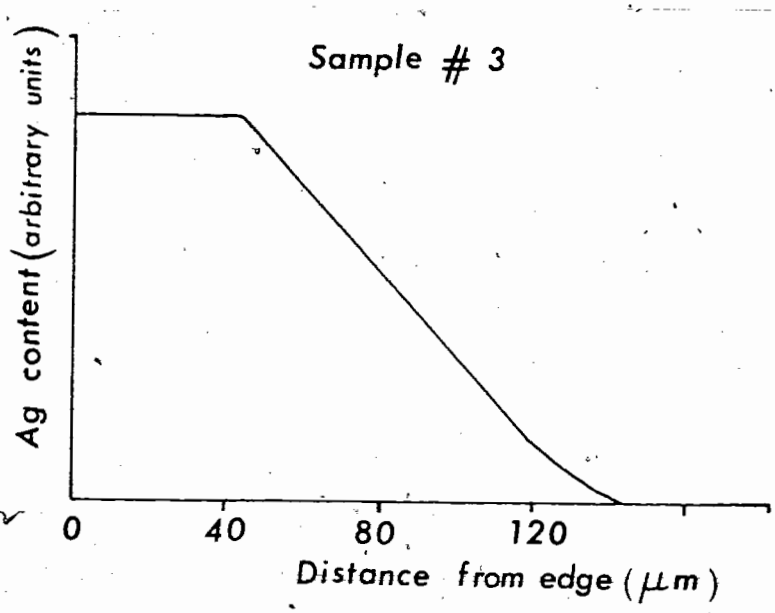
Sample # 3
Ag content (arbitrary units)
0
40
80
120
Distance from edge (μm)

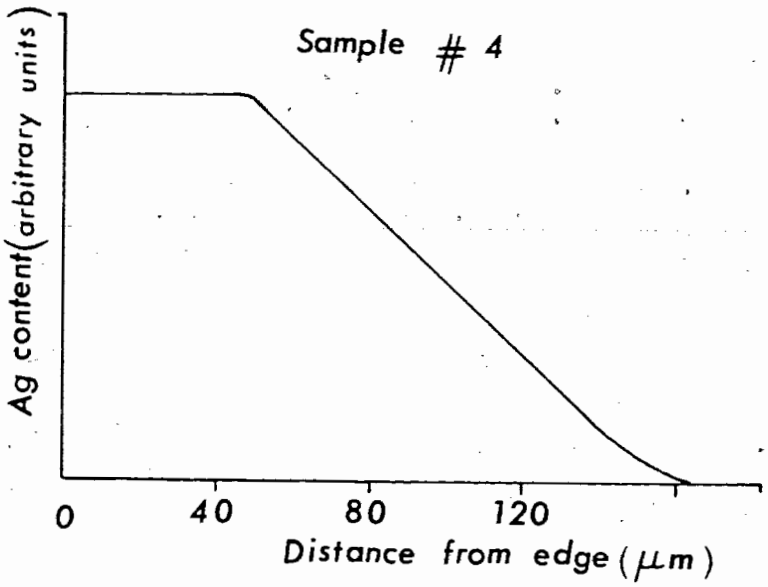
Sample # 4
Ag content (arbitrary units)
0
40
80
120
Distance from edge (μm)

Fig. 4.8

Table 4.4. Results of Ag^{110} tracer experiment : Conversion of stage 1 (Ag^{108}) into stage 2 (Ag^{110}).

Sample # 5

Thickness of the crystal = 4 μm

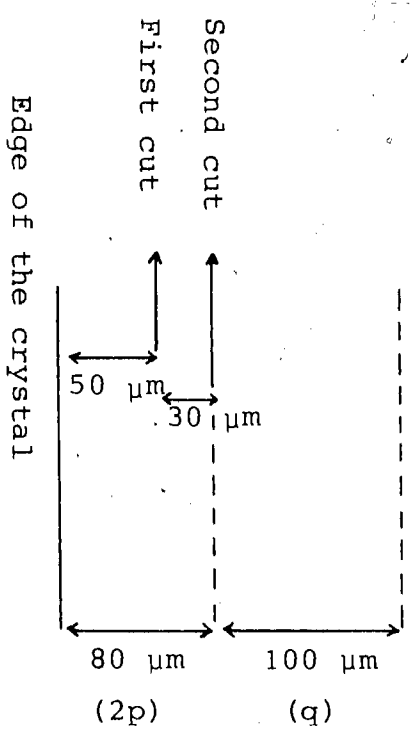

Table 4.4

p ± 5 µm Ag^{108}	q ± 5 µm Ag^{110}	2p ± 10 µm	Counts per second				
			Whole crystal	First cut Width = 50 ± 10 µm		Second cut Width = 30 ± 10 µm	
				Cut off sections	Remaining crystal	Cut off sections	Remaining crystal
40	100	80	10.19 ± 0.23	0.13 ± 0.18	10.02 ± 0.23	1.82 ± 0.19	8.42 ± 0.22

Fig. 4.9. The stage conversion from stage 1 to stage 2 in classical model.

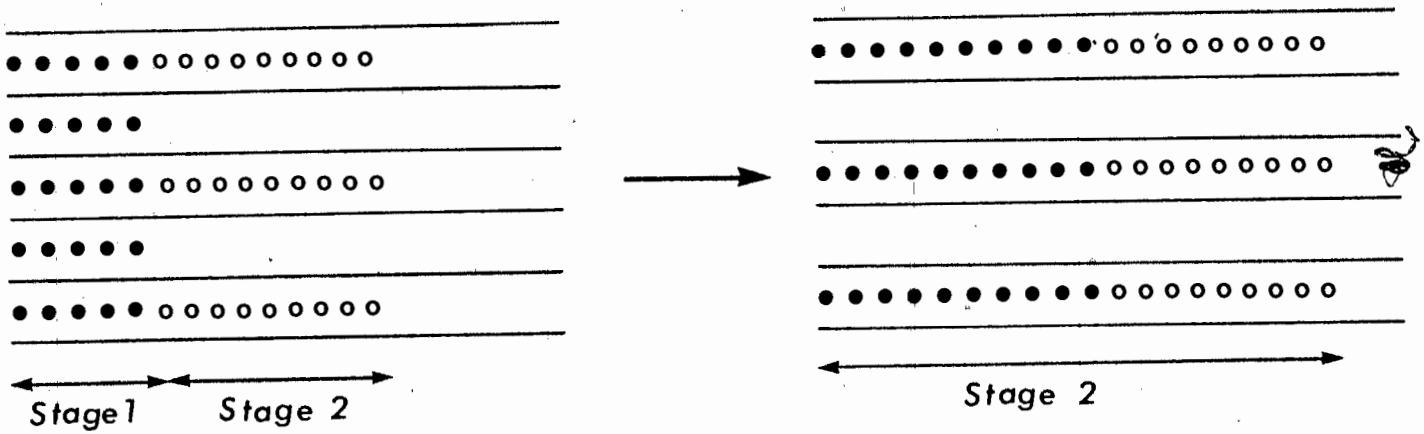

● — Ag^{110}

o — Ag^{108}

Fig. 4.9

Fig. 4.10. Interpretation of results of the tracer experiment in terms of the Daumas and Herold's model.

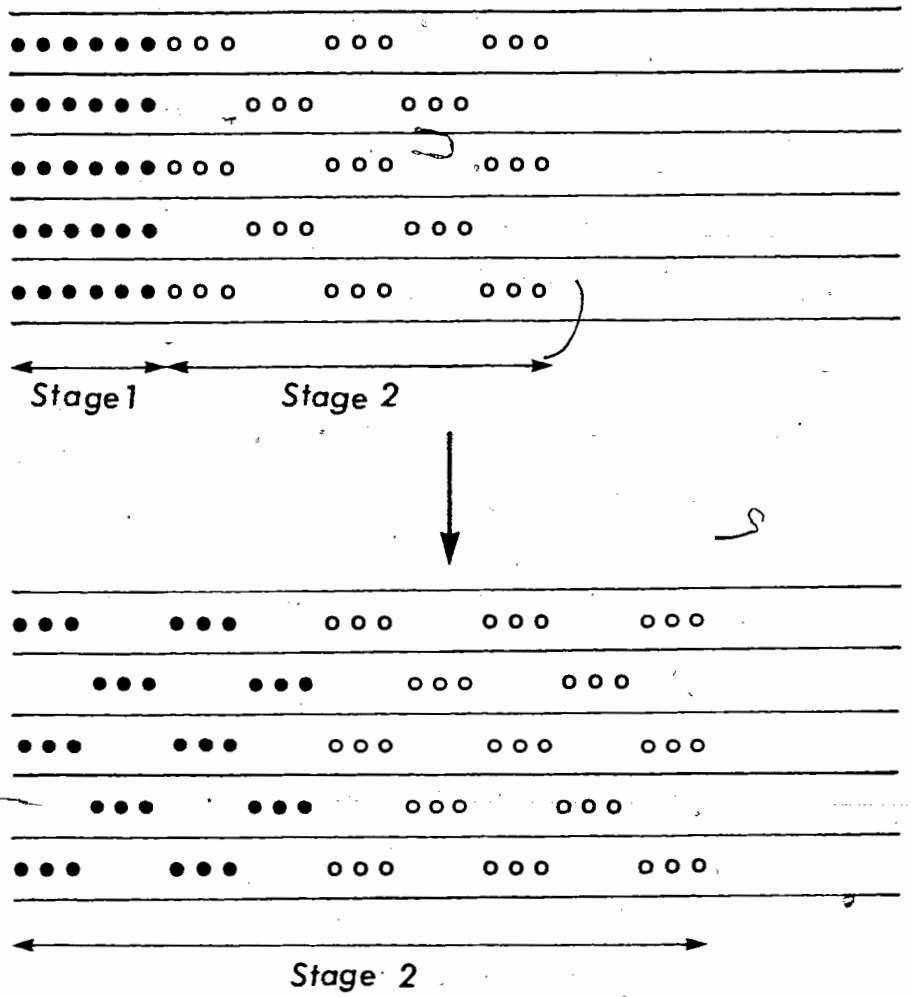

● — Ag^{110}

o — Ag^{108}

Fig. 4.10

V. The island model configuration for intercalation

5.1 Introduction

Daumas and Herold's model or the island model gives a convenient intepretation for various mechanisms that are seen in intercalation compounds. As described in chapter 1 the conversion from a lower stage to a higher is only reasonably described by the island model. The tracer results obtained in chapter 4 were explained with this model without any difficulty while the classical model failed to do so. In the island model it is assumed that the intercalated guest atoms are arranged in two dimensional islands within the Van der Waals gaps. Such islands have never been convincingly observed for any intercalation system. One can suggest different shapes for these islands in the x-y plane such as hexagons, circles, triangles or stripes. When looking at a pure stage 2 region (Fig.5.1) from above, the islands in two adjacent Van der Waals gaps should fill the space without any empty regions. This is not satisfied by hexagonal or circular shaped islands. (Hexagonal islands can be ideally arranged in stage 3.) Triangles can be stacked in a pure stage 2 but the high energy associated with sharp corners would make them unlikely. The striped islands shown in Fig.5.2.(a) appears to be a reasonable possibility for stage 2. Domains of Roman track-shaped islands shown in Fig.5.1 (b) are also a possibility where in a real crystal the domain size may be determined by host stacking faults. It is assumed that the islands for stage 2 silver in TiS have a configuration something like that in Fig. 5.2 (a) or (b) and that the intercalation fronts are like Fig.5.1, the magnitude of the silver island width can be estimated using the XRF data

from chapter 3.

A number of graphs similar to Fig.3.5 (a) and (e) have been obtained for different samples using the XRF microprobe, showing that the intercalation fronts are not sharp. When the final stage 2 front resulting from the stage 1 to stage 2 conversion was stabilized, the width of the front was found to be approximately twice the widths of the stage 1 and initial stage 2 fronts. This can be interpreted using the island model of Fig.5.1. The kinks in the layers in Fig.5.1 are exaggerated since x-ray results showed that the increase in the crystal thickness is about 6.5 % for stage 2 and 13 % for stage 1 (16). Fig.5.1 (a) shows the upper half of a partially intercalated crystal and the lowest layer represents the layer at the middle of the crystal. In the complete crystal the islands are arranged in such a way that the fronts are V-shaped. In Fig.5.1 (a) both the stage 1 and stage 2 intercalated fronts have the same width. The front width doubles as the stage 1 converts to stage 2 as shown in Fig.5.1 (b).

An important result obtained from these diagrams is the relationship between the total number of layers in the crystal and the width of the islands. It is clear in these diagrams that the islands at the intercalation fronts are arranged in steps. Using the widths of the stage 1 or 2 front obtained from the XRF data the width of an island is given by,

$$L = \frac{P}{N/2} = \frac{2P}{N} \qquad \text{for large N,}$$

where,

P = the width of the stage 1 intercalation front and

N = number of host layers in the crystal.

Using the width of the stage 2 intercalation front in Fig.5.3 (b),

$$L = \frac{r}{N} \qquad \text{for large } N,$$

where,

r = the width of the stage 2 front.

N can be calculated for an original crystal of known thickness, using c_o , the c lattice parameter of pure TiS (Fig.1.5 (b)).

5.2 Width of intercalation fronts and calculation of island width

From a number of graphs similar to Fig.3.5 (a) and (e), data for p,q and r in Fig.5.3 were obtained and the island width L was calculated. The results are presented in Table 5.1. The widths of the fronts were determined by fitting the data points at the front to a straight line.

5.3 Discussion

The data for front widths p,q and r obtained with the XRF microprobe given in Table 5.1 are consistent with the diagrams given in Fig.5.3 and Fig.5.1, i.e,the front widths increase with time and r is approximately twice p. Since a finite time was taken (2 1/2 to 3 hrs) to complete a scan across the sample, p and q could not be obtained at the same time. Since the silver in the stage 1 region was moving during this period the value for q could be expected to be a little higher than p. This effect is seen in Table 5.1 and as a result the values for L_q are higher than L_p or L_r .

The average size for L_p and L_r from Table 5.1 are 135 and 130 Å with all of the values lying within 20 % of these values. It should be pointed out here that a change in the width of the front of 3 to 4 μm can change

the L value by 30 to 40 Å and that fitting the data points at the front to a straight line was difficult in some cases. Nevertheless the data of Table 5.1 is quite consistent, so that within the constraints of the model the island width for stage 2 Ag in TiS_2 appears to be of the order of 130 Å.

Fig. 5.1 (a) A partially intercalated crystal : The island model.

l = The width of the pure stage 1 region

p = The width of the stage 1 intercalation front

m = The initial width of the pure stage 2 region

q = The initial width of the stage 2 intercalation front

(b) The crystal after the motion of stage 1 silver.

n = The final width of the stage 2 region

r = The final width of the stage 2 intercalation front

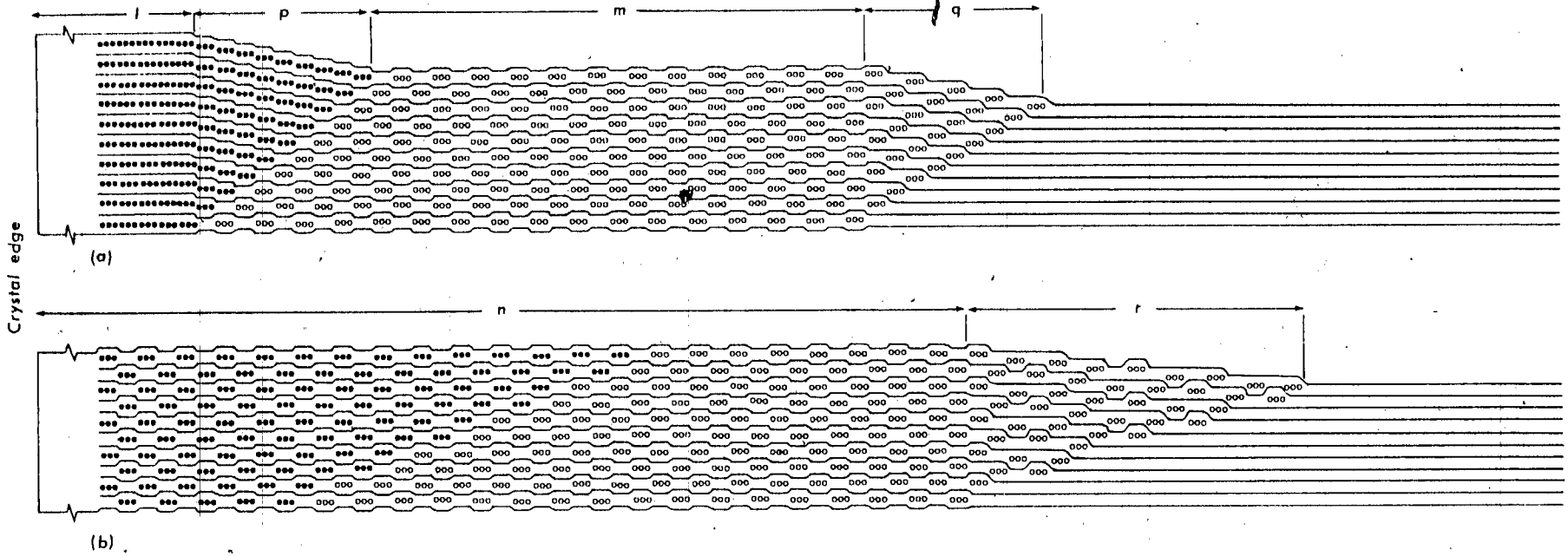

Fig. 5.1

Fig. 5.2. Possible shapes of the islands in stage 2.
(Looking along the c axis)

(a) Striped islands
(b) A domain of Roman track-shaped islands

↑ - islands in an upper layer

↓ - islands in next lower layer

L = the island width

A cross-section of (a) or (b) is same as the stage 2 region given in Fig. 5.1.

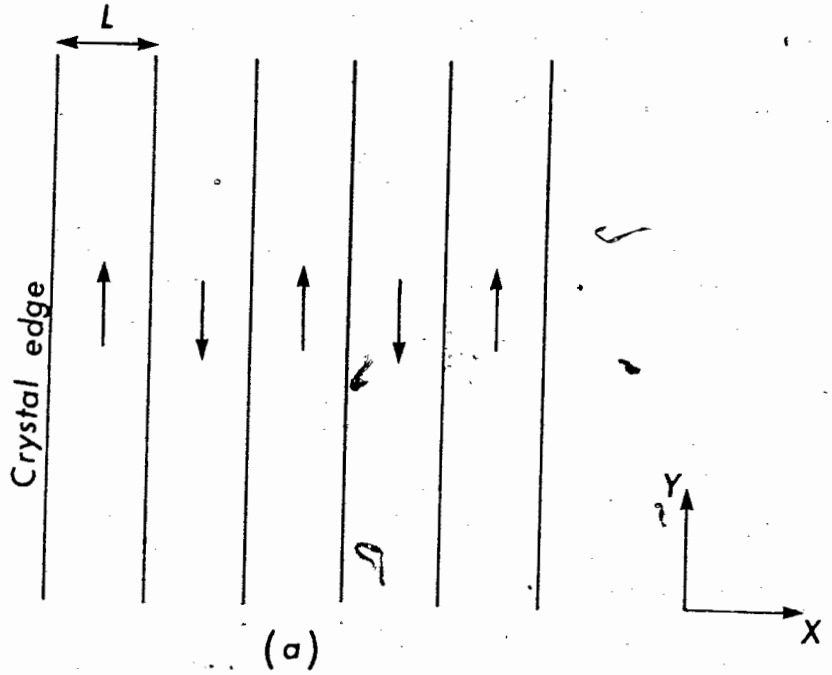

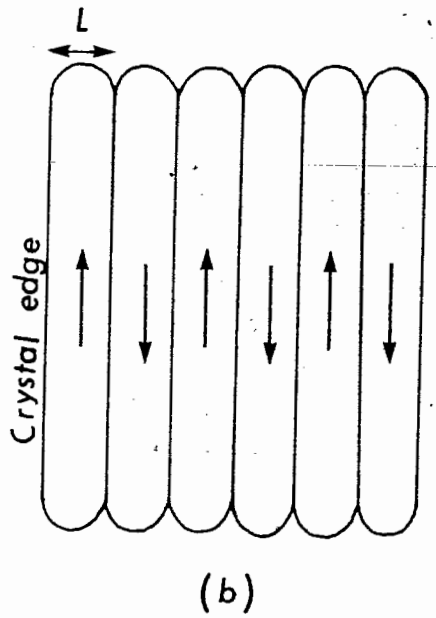

Fig. 5.2

Fig. 5.3. Expected XRF plots for a partially intercalated crystal based on the Ag distribution for Fig. 5.1(a) and (b).

(a) Stage 1 and Stage 2

(b) Stage 2 only

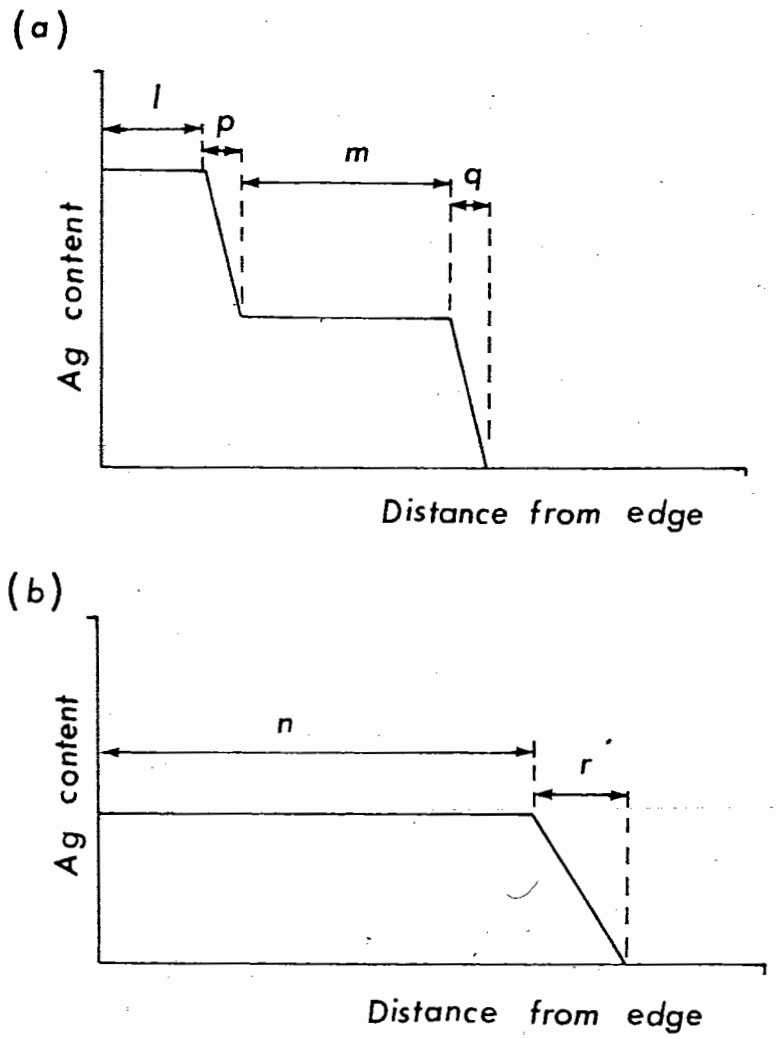
(a)
l
p
m
q
Ag content
Distance from edge
(b)
n
r
Ag content
Distance from edge

Fig. 5.3

Table 5.1. XRF data for front widths and the calculated values for the island width.

* T = Time interval between the start of scanning the corresponding front after stopping the intercalation.

Table 5.1

Thickness ± 0.07 μm	l μm	p μm	m μm	q μm	n μm	r μm	Time (T)* hours			L_p Å	L_q Å	L_r Å
							Stage 1 front (p)	Stage 2 front (q)	Stage 2 front (r)			
0.89	83	12	100	15	265	20	1 1/4	2	After stabilization	155	190	130
1.10	40	13	90	16	170	30	1 1/4	2		135	165	155
1.18	20	15	60	17	100	25	1	1 3/4		145	165	120
1.18	35	13	100	15	170	30	1 1/4	2		125	145	145
2.00	70	22	110	23	255	37	1	2		125	130	105
1.18	85	15	112	20	-	-	1 1/4	2 1/2		145	195	-
1.77	50	20	55	25	-	-	1 1/4	1 3/4		130	160	-
1.47	130	15	210	22	-	-	1 1/4	2 1/2		115	170	-
1.18	-	-	-	-	95	30	-	-		-	-	145
2.00	-	-	-	-	260	38	-	-		-	-	110

VI. Study of the migration of silver perpendicular to the layers of TiS_2

6.1 Introduction

The diffusion of intercalated atoms in layered structures is expected to be highly anisotropic (4). For example a study of diffusion of copper into the layered compound Bi_2Te_3 has shown that the diffusivity in the parallel planes is about eight orders of magnitude greater than the diffusivity in the direction perpendicular to the layers (24).

In this chapter a study of the motion of Ag perpendicular to the layers of TiS_2 lattice is presented. In this experiment, TiS_2 crystals with thin steps were used and only the base part of the crystal steps were intercalated with Ag, supplying a good source of Ag to the step. The silver concentration in the step was determined in the same way as in chapter 3 using the scanning electron microscope with the x-ray fluorescence attachment.

6.2. Sample preparation and intercalation for study of motion of silver perpendicular to the layers

As-grown TiS_2 crystals with thin steps were selected so that in a crystal the height of the step was much smaller than the height of the base crystal. The thicknesses of the steps and the base crystals were measured as outlined in chapter 3 and the thicknesses ranged from 24 to 50 μm for the base crystal and 2.5 to 10 μm for the steps. The crystal mounting was the same as in Fig.3.1 (a) to (e). Then all the edges of the step were covered with a thin layer of RTV to keep silver from entering the step from its edges. Finally the RTV at the corners of the crystal was

covered with graphite dag to avoid charging effects in the electron microscope. Fig.6.1 shows a prepared crystal.

Only the bottom part of the crystal was intercalated with silver using an electrolyte of 0.1 M $AgNO_3$ in glycerol. The sample holder was kept upright and an edge (or two) of the base crystal was wetted with a few drops of the electrolyte such that no part of the step was touching the electrolyte. A small strip of silver was placed into the electrolyte and connected to the graphite block making a short-circuited cell. The base crystals were intercalated for 2 to 5 days depending on the crystal. After the stage 2 front had disappeared underneath the step, the base crystal was further intercalated for another 1 to 3 days giving sufficient time for intercalation of the whole base crystal. The intercalation was stopped before the stage 1 front moved very close to the edge of the step because some crystals cracked with the progress of the stage 1 front. After observing the motion of the intercalation fronts we assumed that the whole base crystal was intercalated providing the step with a good source of Ag. After intercalation the crystal was washed with acetone and taken to the SEM.

6.3 Study of motion of silver perpendicular to the layers of TiS_2

As described in section 3.3 the crystals were scanned along a line perpendicular to the edge of the crystal and the distribution of Ag was determined by XRF for both the exposed base crystal and the step (Fig.6.1). A pure TiS_2 crystal was used as a reference.

A low accelerating voltage (10 kV) was used to reduce the maximum penetration depth of the electron beam. (A high energy electron beam can penetrate through thin steps (chapter 2) down to the base crystal and will give rise to x-rays from the silver in the base crystal.)

Results: The study of motion of Ag at room temperature

All the samples (8 in all) were scanned after intercalation was stopped and it was found that silver had not moved into the steps during the intercalation period (2 to 5 days). Observations during the following two months also gave the same result.

6.4 Study of motion of silver perpendicular to the layers of TiS_2 at 200 °C

Since no motion of silver perpendicular to the layers was observed at room temperature, a sample was heated at 200 °C for one day and the distribution of silver was determined. This was repeated several times for the same sample at the same temperature.

6.5 Results and calculations: The study of motion of silver at 200 °C

After heating the sample, silver was found in the step and the amount of silver increased as the sample was further heated at 200 °C. The results are presented in Fig.6.2.

An estimation for the diffusion coefficient for the motion of silver perpendicular to the layers of TiS_2

The diffusion coefficient for the motion of silver perpendicular to the layers of a TiS_2 crystal at 200 °C was estimated using the graphs in Fig.6.2. The region (3) in Fig.6.2 shows the distribution of silver in the step and the region (1) gives the distribution of silver in the base crystal. Initially the concentration of silver in the step was zero and it increased on heating. The diffusion coefficient was estimated using the

solution (curves in Fig. 6.3) to the 1-dimensional diffusion equation,

$$\frac{\partial c}{\partial t} = D \frac{\partial^2 c}{\partial x^2}$$

where,

C = concentration at a distance x

t = time,

which was first solved by Carslaw and Jaeger (22) as a heat flow problem. The curves in Fig.6.3 are given for a solid with a region $-\ell < x < +\ell$ with zero initial concentration and with the surfaces $x = \pm \ell$ kept at a constant concentration C_o. This case is similar to our case where the region $0 < x < \ell$ is the step and the surface $x = +\ell$ is the top of the base crystal underneath the step.

The concentration distribution at various times in the slab $0 < x < \ell$ is given in Fig.6.3. If it is assumed that the XRF data gives the silver concentration near x = 0 in Fig.6.3, C/C_o can be obtained from the graphs from region (1) and (3) in Fig.6.2. Taking the average readings from curves (b) to (f) in Fig.6.2 and neglecting the area near the edge of the step of region (3), the following values for the diffusion coefficient are obtained: 1.74×10^{-13} , 0.90×10^{-13} , 0.66×10^{-13} , 0.52×10^{-13} and 0.42×10^{-13} cm^2/sec for curves (b) to (f) respectively. It was assumed that the concentration of silver in the base crystal underneath the step was constant (C_o = 0.640) during the heating. Taking a minimum detectable value for C/C_o of about 0.06 (with t = 2 months) the diffusion coefficient at room temperature is estimated to be less than $\sim 10^{-15}$ cm^2/sec.

Graph (b) in region (3) in Fig.6.2 shows that the increase of silver in the step after the first heating is approximately seven times higher

than the increase of silver shown in the graphs (c), (d), (e) and (f). A possible explanation for the reduction of the rate of increase of silver in the step with further heating is that the base crystal under the step is being depleted of silver on heating. Considering the relatively high diffusion along the layers at elevated temperatures the reason for this silver depletion is not clear.

6.6 Discussion

The room temperature study showed that the motion of silver atoms perpendicular to the layers of TiS_2 is negligible.

In the study at 200 °C, only one sample was examined because our main interest was to investigate the possibility of motion perpendicular to the layers at room temperature. Although we do not have data from many samples, we report this data here since the result may be useful for other researchers.

The graphs in region (1) in Fig.6.2 give the silver levels in the exposed base crystal region. It was impossible to obtain data near the edge of the step since that area (region (2)) was covered with RTV (Fig.6.1). The plots in region (3) show the Ag distribution within about 1 μm of the surface of the step. There is a dramatic increase in the amount of silver in the step after the first heating at 200 °C and the amount of silver increased as the sample was heated further. The concentration of Ag in the step decreases slightly with distance in from the edge of the step. This may be due to an initial inhomogeneous concentration of Ag in the base crystal underneath the step.

The graphs obtained for the base part of the crystal are not very well understood. These graphs show an increase of silver at every heating whereas a decrease associated with the filling of the step was expected.

Since a 10 kV electron beam gives the information from a region of about 1 μm deep, the beam probed only 4 % of the thickness of the base crystal. That is, the graphs given in region (1) of Fig.6.2 show the distribution of silver only in the upper layers of the base crystal. The excess silver which is observed in the upper layers of the base crystal could possibly have moved from the lower layers of the base crystal, however the reason for this silver redistribution on heating is not clear.

The results show that the diffusion of silver perpendicular to the layers of the TiS_2 crystal certainly occurs at a sufficiently high temperature. The estimated diffusion coefficient for the motion of silver perpendicular to the layers of TiS_2 at 200 °C is $\sim 10^{-13}$ cm^2/sec and at room temperature it is estimated to be less than $\sim 10^{-15}$ cm^2/sec. This is many orders of magnitude smaller than estimated room temperature diffusion constants of $\sim 10^{-10}$ cm^2/sec for silver along the layers in ultra thin TiS_2 crystals (21) and $\sim 10^{-8}$ cm^2/sec for Li in TiS_2 (4). Such a high anisotropy in the diffusion constant justifies the usual assumption of two dimensional motion for Ag in TiS_2 . A similar anisotropy is to be expected for other intercalated layer compounds.

Fig. 6.1. A schematic diagram of a sample prepared for the study of the motion of silver perpendicular to the layers of TiS_2.

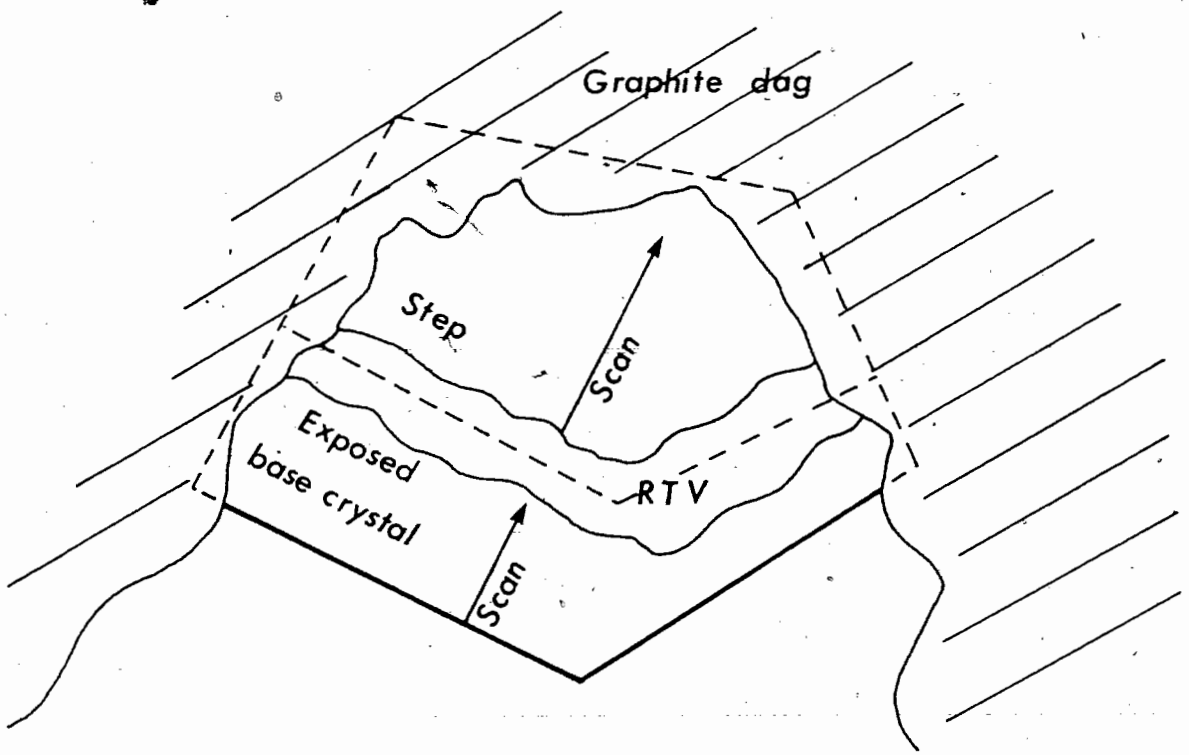

Fig. 6.1

Fig. 6.2. Motion of Ag perpendicular to the layers of TiS_2 at 200 ^{o}C.

Thickness of the base crystal = 24 μm

Thickness of the step = 2.5 μm

(a) ○ - 2 months after intercalation : room temperature

After heating:

		Temperature	Heating time
(b)	▶ -	200 ^{o}C	1 day
(c)	□ -	200 ^{o}C	2 days
(d)	⊗ -	200 ^{o}C	3 days
(e)	△ -	200 ^{o}C	4 days
(f)	● -	200 ^{o}C	6 days

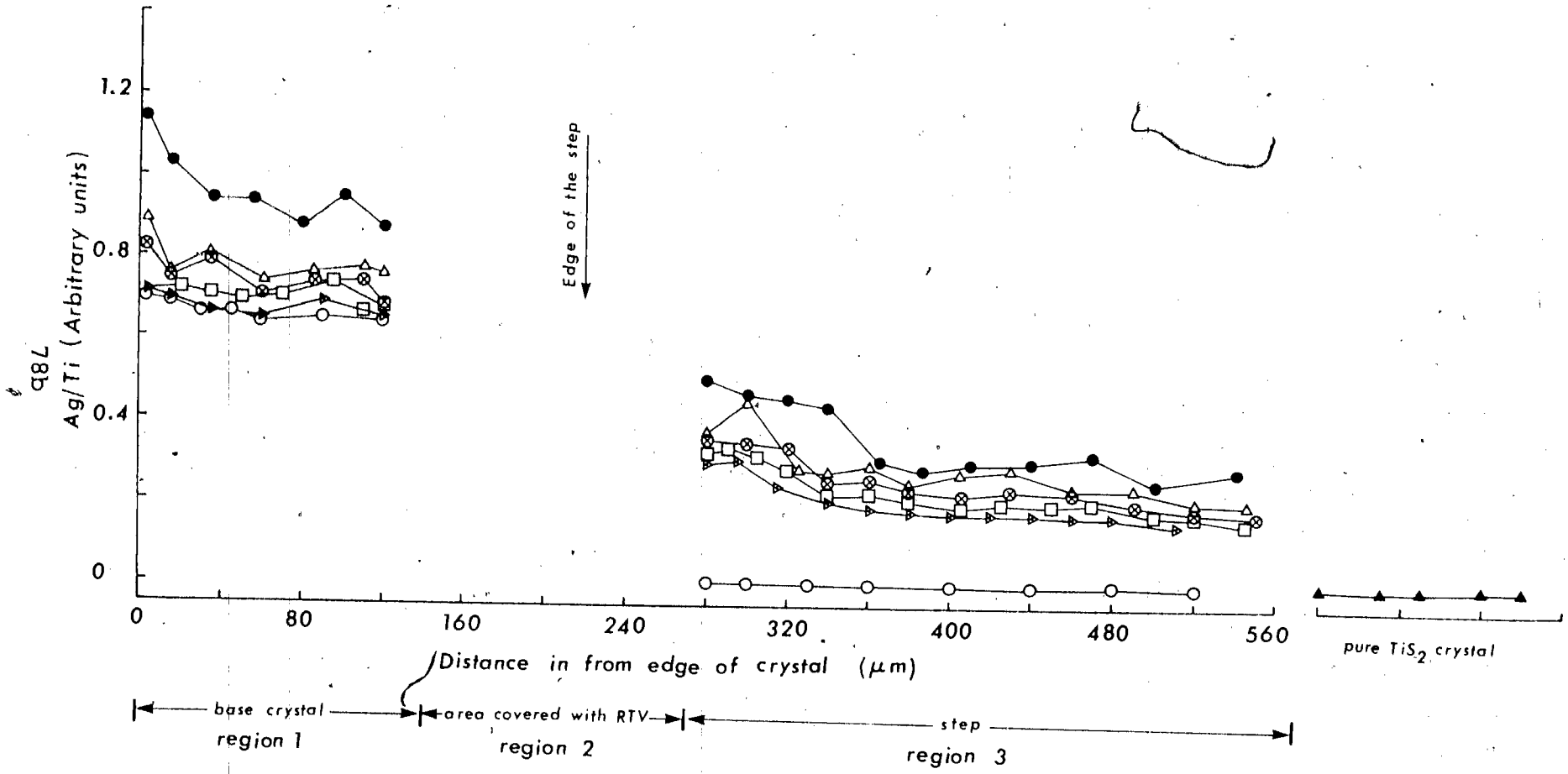
1.2
0.8
0.4
0
Ag/Ti (Arbitrary units)
Edge of the step
0
80
160
240
320
400
480
560
Distance in from edge of crystal (μm)
pure TiS_2 crystal
base crystal
region 1
area covered with RTV
region 2
step
region 3

Fig. 6.2

Fig. 6.3. Concentration distribution at various times in a slab $0 < x < \ell$ with zero initial concentration and a constant surface concentration at $x = \ell$.

The numbers on the curves are the values of

Dt/ℓ^2

Where,

D = diffusion coefficient

t = time

C_o = constant surface concentration at $x = \ell$.

(The solution to the heat flow problem with the same boundary conditions is given in Carslaw and Jaeger, ref. 22.)

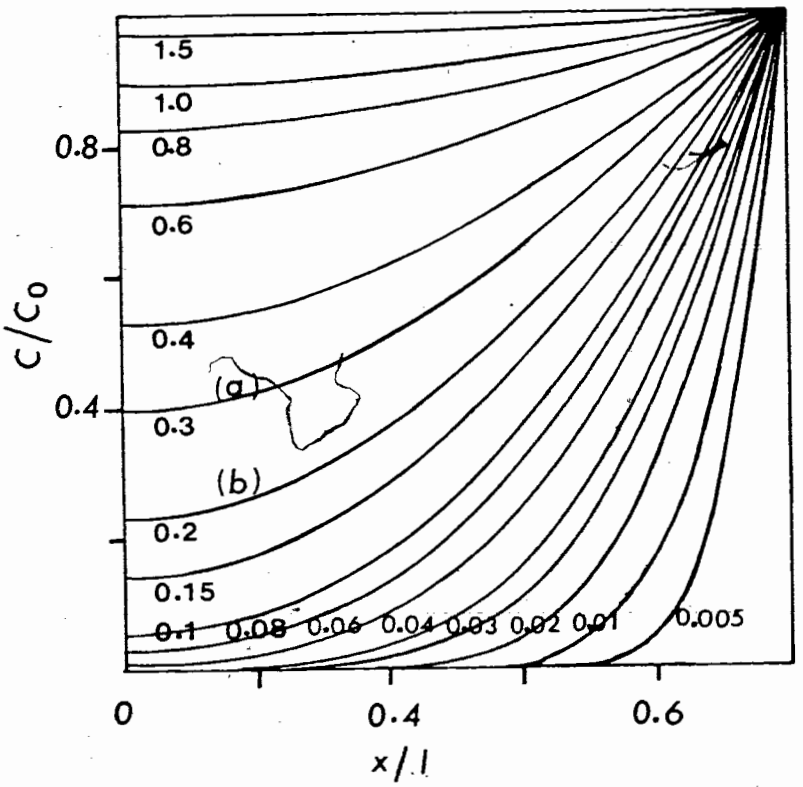
1.5
1.0
0.8
0.6
0.4
0.3
0.2
0.15
0.1
0.08
0.06
0.04
0.03
0.02
0.01
0.005
(a)
(b)
0.8
0.4
C/C0
0
0.4
0.6
x/l

Fig. 6.3

VII. Conclusions

The motion of stage 1 and stage 2 silver in partially intercalated TiS_2 crystals was studied using x-ray fluorescence and it was found that the motion of the stage 1 front occurs rapidly at room temperaure. This process is likely driven by Coulomb repulsive forces between charged silver ions in the stage 1 region.

When stage 1 was not present in the crystal the motion of the stage 2 front was not observed at room temperataure. In the range 200 to 350 °C (depending on the heating time) motion of stage 2 silver does occur, but simple diffusion does not appear to take place.

A radioactive tracer experiment was done to investigate the migration of both stage 1 and stage 2 silver in the TiS_2 lattice at room temperature. It was found that when silver atoms entered a partially intercalated stage 2 crystal most of the newly intercalated silver atoms pushed the preintercalated silver atoms further into the crystal and remained near the crystal edge. When the conversion of stage 1 to stage 2 occurs in a partially intercalated TiS_2 crystal the stage 1 acts as a source of stage 2 islands, and these islands remain near the edge by pushing the stage 2 islands into the interior of the crystal. This motion can be explained by Daumas and Herold's model of staging while the classical model fails to do so.

Using the XRF data and the island model for the intercalation fronts, the width of the islands in stage 2 was estimated to be about 130 Å.

It was observed that, at room temperature the motion of silver perpendicular to the layers is negligible. One sample was studied at 200 °C and migration of silver was observed. The estimated diffusion coefficient for motion of silver perpendicular to the layers in a TiS_2 crystal at

200 °C is $\sim 10^{-13}$ cm^2/sec. At room temperature the diffusion coefficient is estimated to be less than $\sim 10^{-15}$ cm^2/sec.

Bibliography

(1) Whittingham, M.S. and Ebert, L.B., Intercalated Layered Materials, v.6, 533, ed. Levy, F.A., D.Reidel publishing company, Holland (1979).

(2) Levy, F.A., Intercalated Layered Materials, v.1 to 6, D.Reidel publishing company, Holland.

(3) Wilson, J.A. and Yoffe, A.D., Advances in Physics, v.18, 193, (1969).

(4) Whittingham, M.S., Prog. Solid State Chem., v.12, 41, (1978).

(5) Whittingham, M.S. and Gamble, F.R., Mat. Res. Bull., v.10, 363, (1975).

(6) Rudorff, W., Chimica, v.19, 489, (1965).

(7) Safran, S.A. and Hamann, D.R., Phy.Rev.Lett., v.42, 1410, (1979).

(8) Dahn, J.R., Dahn, D.C. and Haering, R.R., Solid State Commu., v.42, 179, (1982).

(9) Milliman, S.E. and Kirczenow, G., Phy. Rev. B (accepted for publication), (1982).

(10) Daumas, N. and Herold, M.A., C. R. Acad. Sci.,Ser. C, v.268, 373, (1963).

(11) Whittingham, M.S. and Panella, J.A., Mat. Res. Bull., v.16, 37, (1981).

(12) Rimmington, H.P.B. and Balchin, A.A., J. of Crystal Growth, v.15, 51, (1972).

(13) Rimmington, H.P.B. and Balchin, A.A., J. of Crystal Growth, v.21, 171, (1974).

(14) Wyckoff, R.W.G., Crystal Structure, v.1, Wiley and Sons, (1963).

(15) Chianelli, R.R., Scanlon, J.C. and Thompson, A.H., Mat. Res. Bull., v.10, 1379, (1975).

(16) Scholz, G.A. and Frindt, R.F., Mat. Res. Bull., v.15, 1703, (1980).

(17) Kittel, C., Introduction to Solid State Physics, John Wiley and Sons, New york, (1976).

(18) Goldstein, J.I. and Yakowitz, H., Practical Scanning Electron Microscopy, Plenum Press, New York, (1977).

(19) Bertin, E.P., Introduction to X-ray Spectrometric Analysis, Plenum Press, New York, (1978).

(20) Good, R.J. and Stromberg, R.R., Surface and Colloid Science, v.2, Ch.6, Plenum Press, New York, (1979).

(21) Scholz, G.A., Joensen, P., Reyes, J.M. and Frindt, R.F., Physica, v.105 B, 214, (1981).

(22) Carslaw, H.S. and Jaeger, J.C., Conduction of Heat in Solids, Oxford, (1959).

(23) Laderer, C.M., Hollander, J.M. and Perlman, I., Table of Isotopes, John Wiley and Sons, New York, (1972).

(24) Carlson, R.O., J. Phy. Chem. Solids, v.13, 65, (1960).